X-chromosome upregulation operates on a gene-by-gene basis at RNA and protein levels

Ryan N. Allsop[1,2,*], Jeffrey Boeren[3,*], Beatrice F. Tan[3,*], Sarra Merzouk[3], Suresh Poovanthingal[2,4], Wilfred F.J. van IJcken[5], Jeroen A.A. Demmers[6], Hegias Mira Bontenbal[3], Cristina Gontan[3], Joost Gribnau[3,#], Vincent Pasque[1,2,#].

[1] Department of Development and Regeneration, University of Leuven (KU Leuven), Leuven, Belgium
[2] KU Leuven Institute for Single Cell Omics (LISCO), Leuven, Belgium
[3] Department of Developmental Biology, Erasmus University Medical Center, Rotterdam, The Netherlands
[4] VIB-KU Leuven Center for Brain & Disease Research, Leuven, Belgium
[5] Erasmus Center for Biomics, Erasmus University Medical Center, Rotterdam, the Netherlands
[6] Proteomics Center, Erasmus University Medical Center, Rotterdam, the Netherlands

* These authors contributed equally: Ryan N. Allsop, Jeffrey Boeren, Beatrice F. Tan
# These authors jointly supervised this work: Joost Gribnau, Vincent Pasque

ABSTRACT

Gene dosage compensation mechanisms are crucial for mammalian development. In mice, recent findings show that cells can sense the number of X chromosomes. Loss or inactivation of one of the two X chromosomes is compensated by upregulating the remaining active X chromosome, a process termed X-chromosome upregulation (XCU). However, how cells sense X-chromosome dosage and induce XCU remains unclear. Here, we show that heterozygous X chromosome fragment deletions in mouse pluripotent stem cells induces XCU *in trans*, and that compensation takes place at the mRNA and protein level. Furthermore, we found that inducing gene silencing *in cis* on autosomes induces gene dosage compensation *in trans*. This work provides significant insights into the molecular foundations of mammalian gene dosage compensation.

INTRODUCTION

Most mammals are diploid, with two copies of each chromosome per cell[1]. In some cases however, the number of chromosomes or segments of chromosomes can change. Changes in gene copy number, also known as changes in gene dosage, have been closely linked to human diseases[2,3]. Gene dosage compensation mechanisms attempt to resolve imbalances in gene dosage[4]. However, how gene dosage compensation is triggered in mammals remains unclear.

A paradigm to study gene dosage compensation mechanisms is the X chromosome. In placental mammals, the female sex is typically characterized by two X chromosomes, while the male sex typically has one X chromosome and one Y chromosome. This imbalance in X-linked gene dosage between sexes is thought to have driven the evolution of X-linked dosage compensation mechanisms[4–11]. In female mammals, one of the two X chromosomes expresses the long non-coding RNA *Xist* and is inactivated *in cis* (on the same chromosome) during early development, a process termed X-chromosome inactivation (XCI)[12,13,14,15]. As a result, there is only one active X chromosome in female somatic cells, while male XY somatic cells also have one active X chromosome. In contrast to the X chromosome, each autosome is present in two active copies. In 1963, Susumu Ohno hypothesized that a dosage compensation mechanism evolved to upregulate X-linked gene expression on the active X chromosome, to balance X-linked gene dosage with the gene dosage of diploid autosomes[9]. This process is referred to as X-chromosome upregulation (XCU)[4]. Recent studies using allele-resolution transcriptome analyses have confirmed that XCU takes place at the transcriptional level in mouse cells with a single active X chromosome, and that XCU is developmentally regulated[4,12,16–34].

Multiple lines of evidence using allele-resolution transcriptome analyses have indicated that mammalian cells can sense the number of X chromosomes they have, as well as the transcriptional status of the X chromosome, and compensate X-linked gene expression accordingly[16,18,20]. Before XCI, female diploid XX mouse pluripotent stem cells (PSCs) have two active X chromosomes (Xa), while male XY cells have only one. By consequence, female mouse PSCs have higher levels of X-linked gene products than male cells. However, recent studies showed that unlike previously thought, each active X chromosome in female XX mouse PSCs and naive epiblast are not upregulated, consistent with no requirement for dosage compensation between two active X chromosomes and diploid autosomes[16,20]. Furthermore, when XX embryonic fibroblasts, with one upregulated active (Xu) and one inactive X chromosome (Xi), are reprogrammed to induced pluripotent stem cells (iPSCs), reactivation of the Xi occurs concomitantly with loss of upregulation from the Xu[16]. A study in mouse iPSCs showed that when one of the two non-upregulated Xa chromosomes is lost in PSCs, XCU is induced on the remaining X chromosome to compensate gene dosage imbalance with diploid autosomes[16]. This observation was later confirmed in mouse embryonic stem cells (mESCs)[20]. Similarly, XCU is also observed in male XY mESCs[20]. In summary, when both X chromosomes are active, there is no XCU. However, when only one active X chromosome is present, XCU is triggered on the remaining active X chromosome.

Collectively, these results suggest that mammalian cells can sense the number of active X chromosomes and compensate for the presence of a single active X chromosome by XCU. However, how cells sense the number of active X chromosomes and trigger compensation for gene dosage imbalances, and if they can sense when specific X chromosome regions or genes are missing, remains unclear.

The molecular mechanisms controlling XCU in mammals are still unknown. Previous studies have attempted to identify active histone modifications associated with XCU in mice, however the results have been conflicting or unclear. One study reported enrichment of histone 4 lysine 16 acetylation (H4K16ac) on the Xu, but analyzed cells with two active X chromosomes, which we now know do not undergo XCU[29]. Another study reported enrichment of histone 3 lysine 4 tri-methylation (H3K4me3) as well as histone 3 lysine 36 tri-methylation (H3K36me3) on the Xu, however this enrichment was compared to autosomes, rather than to the Xa[25]. Finally, a recent study found no enrichment of any common histone modifications on the Xu compared to the Xa[20]. Therefore, it remains unclear whether histone modifications are enriched on the mammalian Xu.

Changes in gene dosage of autosomes is a hallmark of cancer and early human IVF embryos[35–39]. Studies in human cancer cells and human embryos have suggested that gene dosage compensation can occur on autosomes at both the transcriptional and translational levels[35,40]. However, it is unknown if these effects can also be induced by gene silencing on an autosome, as opposed to genetic loss.

In this study, we sought to investigate how the X chromosome and autosomes sense and compensate for changes in gene dosage in mammals. We use CRISPR-Cas9 to generate large heterozygous X-linked deletions in female XX mESCs, followed by allele and molecule-resolution single-cell and bulk transcriptomics, as well as quantitative proteomics to measure the impact of the deletions on gene expression. We find evidence for dosage compensation by increased transcription and protein levels specifically within the deleted regions *in trans*. Furthermore, we investigated whether dosage compensation of autosomal genes can occur without loss of genetic material, and found evidence for transcriptional dosage compensation *in trans* (on the other chromosome) when one of two alleles is inactivated *in cis*. In conclusion, this work establishes that mammalian cells can sense the heterozygous loss or inactivation of specific fragments of chromosomes or genes and compensate these gene dosage imbalances by upregulation at the transcriptional and protein levels *in trans*.

RESULTS

Allele and molecule-resolution analysis of XCU in mouse PSCs

To investigate XCU, we used single-cell RNA-sequencing (scRNA-seq) in mouse PSCs with a range of genotypes. The cell lines originate from a cross between two mouse subspecies (*Mus musculus musculus* x *Mus musculus castaneus*, *Mus/Cast*). The cells were 1) female iPSCs with two active X chromosomes ($X^{Cast}X^{Mus}$), 2) male ESCs ($X^{Mus}Y$) and 3) female mESCs with X-chromosome monosomy of the paternal or maternal X chromosome (XO,

115 either $X^{Cast}O^{Mus}$ or $X^{Mus}O^{Cast}$) (**Figure 1a**, **Supplementary Fig. 1a**)[41]. Previous studies
116 indicated that both mESCs and iPSCs behave similarly with respect to X chromosome
117 dosage compensation properties[16,20,41–43]. We applied Smart-seq3xpress, a plate-based
118 scRNA-seq method providing full transcript coverage with the ability to count the number of
119 transcript molecules using unique molecular identifiers (UMIs)[44]. Transcripts were further
120 split by allele of origin based on a list of ~17.5 million single-nucleotide polymorphisms
121 (SNPs) unique to each subspecies[16,45,46], providing allele-specific resolution data.

122 To quantify gene expression from each X chromosome, we measured the mean normalized
123 expression (transcripts per million, TPM) of all expressed X-linked genes from each allele for
124 each cell line. This enabled us to identify which X-chromosome was lost in the XO cells
125 (**Supplementary Fig. 1b**). XX iPSCs and ESCs have been previously described to lose one
126 of the two X-chromosomes[41,43,47,48]. Consistent with this, after quality filtering, we obtained 6
127 cells which lost the *Cast* allele ($X^{Mus}O^{Cast}$), and 44 cells which lost the *Mus* allele ($X^{Cast}O^{Mus}$).
128 As expected, we observed significantly higher allelic expression levels when only one active
129 X chromosome is present, in $X^{Mus}Y$ and $X^{Mus}O^{Cast}$ cells (**Figure 1b**, **Supplementary Fig. 2a**).
130 When the *Mus* allele rather than the *Cast* X chromosome allele was lost, in $X^{Cast}O^{Mus}$ cells, X-
131 linked gene expression was increased on the *Cast* allele (**Figure 1c**). In summary, loss of
132 one X chromosome in XX mouse PSCs induces global compensation of gene expression on
133 the remaining monosomic X chromosome. Allelic X-to-autosome ratio (X:A) analysis
134 confirmed elevated X:A ratios in cells with a single X chromosome, while $X^{Cast}X^{Mus}$ cells
135 exhibited no increased X:A ratio, confirming previous findings[16,20] (**Figure 1d-e**,
136 **Supplementary Fig. 2b**). These findings confirm the presence of XCU in diploid cells with
137 a single X chromosome[16], and that mouse PSCs can sense the number of X chromosomes
138 and adapt gene expression by undergoing XCU when only one Xa is present. Consistent
139 with previous studies, the average expression from the *Mus* allele tended to be slightly
140 higher than the *Cast* allele, a slight bias most likely induced to mapping reads to the *Mus*
141 *musculus musculus* reference genome[16,18,49]. Together, these results confirm that
142 transcriptional dosage compensation by XCU occurs in mouse PSCs with a single active X
143 chromosome, but not with two active X chromosomes. Moreover, we can accurately
144 measure and identify XCU using a hybrid/polymorphic mouse PSC system combined with
145 allele-specific expression analysis using Smart-seq3xpress scRNA-seq.

146

147 **Identification of genes subject to XCU**

148 We next sought to characterize which X-linked genes are transcriptionally dosage
149 compensated in this system. Of the 405 expressed X-linked genes for which we obtained
150 allele-resolution expression data, 103 (~40%) were found to be significantly transcriptionally
151 upregulated in XO and XY cells (collectively $X^{monosomy}$) compared to XX cells (**Supplementary**
152 **Fig. 2c, Supplementary Table 1**). These results are in line with previous findings that
153 transcriptional XCU is specific to a subset of genes[17]. Both non-upregulated and
154 upregulated genes were found to be located across the X chromosome and not enriched to
155 a specific locus (**Supplementary Fig. 2d**). The mean allelic expression of the upregulated
156 genes was significantly higher in $X^{monosomy}$ cells than in XX cells (**Supplementary Fig. 2e-h**).

To characterize the expression levels of genes subject to XCU in cells that do not undergo XCU, we compared in XX cells the mean expression of genes defined as upregulated and non-upregulated. We found that genes that are upregulated in $X^{monosomy}$ are expressed at significantly higher levels in XX iPSCs compared to genes that are not subject to upregulation in $X^{monosomy}$ (**Figure 1f**). This is in line with previous findings that highly expressed genes are also more likely to be dosage-sensitive[50], and that dosage compensation mechanisms have evolved primarily to protect dosage-sensitive genes from the harmful effects of gene dosage imbalances[51].

Interestingly, gene ontology analysis indicated that upregulated X-linked genes were enriched for critical basic cellular functions such as regulation of chromatin organization and positive regulation of nucleic-acid templated transcription, whereas non-upregulated genes were enriched for specific developmental processes such as visual perception and negative regulation of axonogenesis, processes that are irrelevant at this stage of development (**Supplementary Fig. 2i**). Proteins encoded by upregulated genes were more likely to have protein-protein interactions (PPIs) with transcription factors, which could be due to feedback loops which allow upregulated genes to self-regulate their expression (**Supplementary Fig. 2j**)[52]. Genes encoding proteins that form complexes have been hypothesized to be particularly dosage-sensitive, potentially requiring gene dosage compensation in order to maintain the correct stoichiometry for proper complex function[51,53]. However, despite an apparent trend, our upregulated X-linked genes did not contain a significantly higher proportion of genes which code for proteins in complexes when compared to non-upregulated X-linked genes (**Supplementary Fig. 2k**). Examples of important complexes containing subunits encoded by upregulated genes include the MLL1, MSL, NSL, and DNA polymerase complexes, which contain subunits respectively encoded by *Hcfc1*, *Msl3*, *Ogt*, and *Pola1* genes.

Proteins which form condensates have been proposed to be particularly dosage-sensitive[54]. However, we found no significant difference in the proportion of proteins forming condensates between upregulated and non-upregulated genes, indicating that transcriptionally upregulated X-linked genes may not be enriched for genes encoding proteins known to form condensates (**Supplementary Fig. 2l**). Given the challenges in studying condensates, it remains possible that not all condensate-forming proteins have been identified, and future discoveries may revise this conclusion[55]. Furthermore, we hypothesized that genes which escape XCI, and thus retain expression from both alleles, require dosage compensation in $X^{monosomy}$ cells. We observed a non-significant trend towards an increased proportion of upregulated genes that escape XCI (**Supplementary Fig. 2m**), potentially due to the limited statistical power from the small escapee gene set (n=38)[56]. Nearly all orthologs of the upregulated X-linked genes were associated with diseases in the OMIM database, however, this proportion was not significantly higher than that of the non-upregulated genes (**Supplementary Fig. 2n**). Taken together, these results suggest that upregulated genes may be dosage-sensitive, and this may be linked to high levels of gene expression, involvement in protein complexes, and important cellular function.

199

200 **Histone post-translational modifications and XCU**

201 To explore a potential link between histone post-translational modifications (hPTMs) and
202 XCU, we analyzed hPTMs in a system that enables conditional induction of XCU in mouse
203 XX ESCs[57]. In the study of Zylicz et al.[57], a doxycycline inducible promoter was inserted
204 upstream of the endogenous *Xist* gene on the *Mus* allele in polymorphic ($X^{Cast}X^{Mus}$) mESCs[57].
205 Addition of doxycycline for 24 hours activates *Xist* on the *Mus* allele, inducing XCI *in cis*,
206 and triggers XCU on the opposite active X^{Cast} chromosome *in trans*[20]. Therefore, this
207 experimental system enables us to examine hPTMs during XCU. To assess the enrichment
208 of various hPTMs, we examined native ChIP-seq data with allele resolution for several
209 hPTMs (H4ac, H3K27ac, H3K4me1, H3K4me3, H3K9ac, H3K27me3, H2AK119ub) at 0, 4,
210 12, and 24 hours of XCI and XCU induction with allele resolution (**Figure 1g**). As expected,
211 during XCI, there was an increase in repressive marks H3K27me3 and H2AK119ub at the
212 promoter region and across the gene body of X-linked genes on the Xi (**Supplementary**
213 **Fig. 3a-c**). By contrast, on the Xa during XCU, there was no increase in the repressive
214 mark H3K27me3 and minor increase in H2AK119ub in the promoter regions (**Figure 1h,**
215 **Supplementary Fig. 3d**). Across the gene body, there was a significant decrease in
216 H3K27me3 and a small but protracted increase in H2AK119ub on the Xa during XCU
217 (**Supplementary Fig. 3d-e**). Additionally, active marks decreased in the promoter region of
218 genes on the Xi (**Supplementary Fig. 4a-b**). However, on the Xa, H4ac, H3K27ac,
219 H3K4me1, and H3K4me3 remained high, while H3K9ac significantly increased during XCU
220 (**Figure 1i, Supplementary Fig. 4c**). These results indicate that while active marks become
221 depleted during XCI, a subset of active hPTMs become more enriched during XCU, or
222 remain high (**Supplementary Fig. 4d**). Our results implicate these hPTMs in XCU in
223 mammals in contrast to the recent view that they are not enriched on the Xu[20,25,29,41].

224 In addition, we found that before XCU, all active marks studied are more highly enriched on
225 genes that will become upregulated during XCU versus those that do not, in line with the
226 higher expression levels of these genes before XCU (**Figure 1i, Supplementary Fig. 4c**).
227 Unlike a previous study[20], we find evidence for an increase in several active hPTMs during
228 XCU. This could be because the changes we detected are restricted to the promoter
229 region. A previous study did propose increased hPTM on the Xu in XX mESCs[25], but given
230 we now know XX mESCs have no XCU, the conclusions from this study must be revisited.
231 By contrast, strong evidence has been provided for a role of H4K16ac in XCU in *Drosophila*
232 *melanogaster* where the male-specific lethal (MSL) complex deposits H4K16ac on the Xu[58].
233 To investigate if mammals and *Drosophila* both acquired mechanisms to enrich H4K16ac
234 on the Xu, we investigated whether H4K16ac is enriched on the Xu in mice. A previous
235 study analyzed acetylated H4 (H4ac) in mESCs but did not identify any enrichment on the
236 Xu, the pan-H4ac detection potentially masking H4K16ac enrichment[57]. We therefore
237 performed H4K16ac ChIP-seq in both XX and XO mESCs, which showed no significant
238 increase in H4K16ac on the Xu compared to the Xa (**Supplementary Fig. 4e-f**). In
239 summary, we found evidence for enrichment of active hPTMs during XCU in mammals
240 similar to *Drosophila*. However, different sets of histone marks appear to be enriched on the
241 Xu in different species, H4K16ac in *Drosophila*[58], and H3K9ac in mice.

242 **No evidence for an XCU center**

243 To gain insights into how cells sense the number of active X chromosomes they carry and
244 subsequently induce XCU, we hypothesized the existence of a dedicated regulatory locus
245 on the X chromosome, which we term the XCU center (Xuc). By analogy to the well-
246 characterized X-inactivation center (Xic)[8,14,59], the Xuc is defined as an X-linked locus whose
247 loss or inactivation on one allele leads to chromosome-wide upregulation of gene
248 expression *in trans* on the other X chromosome (**Figure 2a**). We propose that the presence
249 of two active copies of the Xuc prevents XCU, whereas having only one active copy is
250 necessary to induce XCU. Specifically, when both Xuc copies are active (two Xa), no XCU
251 occurs; when one Xuc is active and the other is inactive or absent (one Xa), XCU is induced
252 on the Xa. To test the Xuc hypothesis, we investigated the impact of deleting large
253 segments on one of the two X chromosomes in XX mESCs on gene expression. We
254 wondered if deleting a large segment or region on one of the two X chromosomes would be
255 sufficient to induce chromosome-wide XCU *in trans*.

256 We used XX mESCs with large heterozygous segmental deletions on one of the two X
257 chromosomes. The cell lines were 1) Deletion 1: a 49 Mb deletion between *Tfe3* and *Zic3*, 2)
258 Deletion 2: a 15 Mb deletion between *Zic3* and *Dusp9*, and 3) Deletion 3: a 15 Mb deletion
259 of the region between *Dusp9* and *Nr0b1* (**Figure 2b**, **Supplementary Table 2**)[41]. We also
260 included $X^{Cast}X^{Mus}$ iPSCs, $X^{Cast}O^{Mus}$ iPSCs, $X^{Mus}O^{Cast}$ iPSCs and $X^{Mus}Y$ ESCs as controls and
261 performed Smart-seq3xpress scRNA-seq as above. After quality filtering, we obtained
262 allele-resolution expression values for 405 X-linked and 12,016 autosomal genes in 325
263 cells. ScRNA-seq data confirmed the genotype of the cells (**Figure 2c**). All cell lines
264 expressed pluripotency markers, indicating that cells maintained a pluripotent stem cell
265 identity (**Supplementary Fig. 5a**). Correlation analysis confirmed that the heterozygous
266 deletions did not affect the transcriptome, as indicated by the strong correlation between all
267 cell lines (**Supplementary Fig. 5b**). In summary, we generated allele-resolution scRNA-seq
268 data for polymorphic PSCs with distinct heterozygous deletions of the X chromosome.

269 We first asked if deleting a large segment on one of the two active X chromosomes results
270 in induction of global XCU *in trans*. Allele-specific gene expression analysis showed that
271 none of the three deletions examined induced full global XCU *in trans* (**Supplementary Fig.**
272 **5c-f**). However, we noted a slight increase in gene expression *in trans* in two cell lines,
273 Deletion 1 and 3, but the magnitude of the increase was low. To understand where this
274 increase may come from, we first analyzed gene expression specifically outside of the
275 deleted segments *in trans* (**Figure 2d**). While full loss of one of the two X chromosomes
276 induces XCU, none of the segmental deletions induced full XCU *in trans* for genes located
277 outside of the deletion segments (**Figure 2e-g, Supplementary Fig. 5g-j**).

278 To determine if the conclusions can be extended to other regions of the X chromosome, we
279 proceeded to test deletions that collectively span the entire X chromosome. We generated
280 13 new individual large segmental heterozygous deletions of the X chromosome in $X^{Cast}X^{Mus}$
281 mESCs (**Figure 3a**, **Supplementary Fig. 6a**, **Supplementary Table 2**). This included ten
282 deletions, labeled A to K, as well as three larger deletions spanning multiple regions (AB, C-
283 G, I-TEL). Deleted segments were chosen to respect syntenic segments and TAD

284 boundaries[60] as much as possible (**Supplementary Fig. 6b**). These deletions were
285 generated in a *Rnf12*$^{+/-}$ parental cell line, which exhibits highly similar expression to wild
286 type XX mPSCs as expected (**Supplementary Fig. 6c**), and thus served as the reference
287 sample for these analyses. We generated bulk RNA-seq data from two independent clones
288 from most deleted lines. We used $X^{Cast}X^{Mus}$, $X^{Mus}O^{Cast}$, and $X^{Cast}O^{Mus}$ mESCs as controls. After
289 quality filtering, we obtained expression values for 447 X-linked and 11,203 autosomal
290 genes, enabling us to investigate X-linked gene dosage compensation. Allele-resolution
291 analysis of X-linked gene expression confirmed the expected genotype of the cells (**Figure**
292 **3b**). Pluripotency gene expression was maintained (**Supplementary Fig. 6d**). The
293 heterozygous deletions did not affect the global transcriptome, as confirmed by a
294 correlation analysis between all sequenced samples (**Supplementary Fig. 6e**). These
295 results confirm the successful generation of a high-quality dataset of deletions spanning the
296 entire X chromosome, suitable for testing the Xuc hypothesis.

297 As expected, XX cells had higher X-linked gene expression levels compared to XO cells
298 (**Supplementary Fig. 6f**). However, when gene expression is normalized per X
299 chromosome, XO cells showed XCU (**Figure 3c**). In contrast, none of the 13 new deletions
300 induced global full XCU for genes located outside of the deleted regions. At the gene level,
301 genes upregulated in $X^{Cast}O^{Mus}$ cells remained expressed at lower levels outside the
302 deletions across all deletion lines compared to $X^{Cast}O^{Mus}$ cells (**Figure 3d**). None of the
303 deletions caused significant expression changes relative to $X^{Cast}X^{Mus}$, with the exception of
304 deletion AB. This likely represents an outlier, as deletion of region A or B alone had no
305 significant effect, and the magnitude of change for AB was smaller than in $X^{Cast}O^{Mus}$ cells. In
306 summary, deletion of large segments on one of the two X chromosomes is not sufficient to
307 induce full XCU outside of the deleted regions. Collectively, these results do not support the
308 hypothesis that any of the segments deleted act as an Xuc with the ability to induce global
309 XCU of the X chromosome *in trans*.

310

311 **Cells sense large segmental deletions and compensate gene expression *in trans***
312 To test if large segmental deletions are compensated within the deleted regions *in trans*, we
313 examined XCU specifically within deleted segments (**Figure 4a**). Remarkably, there was a
314 strong induction of XCU specifically within deleted segments *in trans* (**Figure 4b-d**,
315 **Supplementary Fig. 7a-c**). Moreover, the level of XCU was similar to that of XO cells in
316 most cell lines. We made similar observations for the 13 segmental deletions of the X
317 chromosome, in which XCU was induced within deleted segments *in trans* (**Figure 4e**,
318 **Supplementary Fig. 7d**). To quantify XCU at the gene level, we examined expression
319 levels of genes upregulated in $X^{Cast}O^{Mus}$ cells relative to $X^{Cast}X^{Mus}$. These genes were
320 consistently upregulated across the deletion lines, reaching expression levels similar to
321 those in $X^{Cast}O^{Mus}$ cells (**Figure 4f**). Allele-specific analysis confirmed upregulation of the
322 *Cast* allele in $X^{Cast}O^{Mus}$ cells (**Supplementary Fig. 7e**). These results demonstrate that
323 mammalian cells can sense when specific segments of one of the two X chromosomes are
324 genetically deleted and compensate for gene dosage imbalances by transcriptional
325 upregulation specifically *in trans*.

Next, we aimed to define if the upregulated genes within the deleted regions in the deleted lines are the same as the upregulated genes in XO cells. To address this, we asked if genes upregulated in XO cells were also upregulated when deleted in cells with large heterozygous deletions. We found that 64 of the 65 upregulated genes located within deletions 1-3 were also upregulated in each of the deletions *in trans* (**Figure 4g**). Likewise, genes upregulated in cells with deletions were also upregulated in cells with $X^{monosomy}$ (**Supplementary Fig. 7e**). This high degree of overlap suggests a shared transcriptional response to X chromosome dosage loss.

These results favor a model in which specific regions or even individual genes can sense gene dosage and even gene expression states and adapt X-linked gene expression accordingly by XCU. We investigated whether deletion of a single allele of a gene would also result in transcriptional dosage compensation of that gene *in trans*. In other words, we asked if one allele of a gene can sense and respond to deletion of the other allele *in trans*. We focused on a single gene, *Pdzd4*, that is subject to XCU, and generated mESCs which contain a heterozygous deletion of the promoter and gene body of *Pdzd4* on the *Mus* allele (**Supplementary Fig. 7g**). Allele-specific quantitative PCR analysis indicated upregulation *in trans* for three of the four clones heterozygous for *Pdzd4* (**Figure 4h**). These results suggest that *Pdzd4* is transcriptionally compensated *in trans* when one of the two alleles of *Pdzd4* is deleted. We conclude that heterozygous loss of a gene body and corresponding promoter on the X chromosome can be sensed and compensated via increased transcription in *trans*.

Autosomal gene dosage compensation by transcriptional upregulation *in trans*

So far we have provided evidence for transcriptional compensation of monosomies of the X chromosome *in trans*, consistent with the evolution of dosage compensation mechanisms on the X chromosome by XCU[4–11]. Next, we aimed to determine if dosage compensation by transcriptional upregulation *in trans* can take place on autosomes. To explore autosomal gene dosage compensation, we used a bulk RNA-seq dataset of *Mus/Cast* mESCs with inducible autosomal gene silencing *in cis*[61]. In this system, addition of dox activates an inducible *Xist* transgene inserted on the *Cast* allele of chromosome 3, resulting in the transcriptional downregulation of many genes *in cis* on that allele (**Figure 5a, Supplementary Fig. 8a**)[61]. This experimental setting enabled us to ask if reduction of autosomal gene expression *in cis* induces dosage compensation *in trans*. We confirmed reduced gene expression *in cis* and identified a ~80 Mb region with a high density of genes that decrease expression on the *Cast* allele after *Xist* expression for 24 hours (**Figure 5b-c**). To assess gene-by-gene compensation, we first examined genes located outside of the 80-160 Mb region *in trans*, on the *Mus* allele, and did not detect changes in gene expression (**Figure 5d**). By contrast, inducing reduced gene expression of chromosome 3 *in cis* induced significant transcriptional upregulation of the corresponding *Mus* allele *in trans* in the 80-160 Mb region (**Figure 5e**). Contrary to our findings on XCU, the baseline expression level prior to addition of doxycycline was significantly lower for upregulated genes

368 compared to non-upregulated genes (**Supplementary Fig. 8b**), potentially due to the fact
369 that the expression of highly expressed genes is not sufficiently reduced in this
370 experimental system. Upregulated chromosome 3 genes were not enriched for genes which
371 encode proteins in complexes, or proteins which form condensates (**Supplementary Fig.**
372 **8c-d**). In summary, we found that decreasing expression *in cis* resulted in upregulation *in*
373 *trans* for several genes on chromosome 3 after 24 hours of doxycycline. Therefore, these
374 results suggest that reducing expression of autosomal genes *in cis* can be compensated by
375 transcriptional upregulation *in trans*.

376

377 **Gene dosage compensation at the protein level**

378 XCU has been described to occur at the transcriptional level in mouse embryos and ESCs
379 but its occurrence at the protein level in mouse PSCs remains to be established[16,17,20,62]. To
380 determine if XCU takes place at the protein level in XO and XY ESCs, we performed
381 quantitative proteomics in $X^{Cast}X^{Mus}$, $X^{Mus}Y$, and $X^{Cast}O^{Mus}$ ESCs. We also included two ESC
382 lines with large heterozygous segmental deletions (Deletions E and K), which showed high
383 percentages of transcriptionally upregulated genes located within the deleted region
384 (**Supplementary Table 2**). We identified 8,050 proteins, of which 4,446 proteins were
385 detected in all samples.

386 We next analyzed X-linked protein levels and found them to be more abundant in $X^{Cast}X^{Mus}$
387 ESCs compared to $X^{Mus}Y$ and $X^{Cast}O^{Mus}$ cells, in agreement with increased X-linked gene
388 expression in these cells due to the presence of two active X chromosomes
389 (**Supplementary Fig. 9a**). Since mass spectrometry results do not provide allelic
390 resolution, we normalized protein abundances for the X-chromosome copy number. On a
391 per-X-chromosome basis, XCU was detected at the protein level in $X^{Mus}Y$ and $X^{Cast}O^{Mus}$
392 ESCs compared with $X^{Cast}X^{Mus}$ ESCs (**Figure 6a**). Indeed, ESCs with one active X
393 chromosome showed more than half of X-linked protein abundances, suggesting XCU at
394 the protein level (**Supplementary Fig. 9a**). The increase was also seen for the X:A ratio
395 (**Supplementary Fig. 9b**). Therefore, we confirm that XCU takes place at the protein level
396 in $X^{Mus}Y$ and $X^{Cast}O^{Mus}$ ESCs to compensate for the absence of one of the two active X
397 chromosomes. These results show that the single active X chromosome of mESCs is
398 upregulated at the protein level compared to each X chromosome in XX mESCs.

399 We next examined which proteins are subject to upregulation in ESCs with only one active
400 X chromosome. Focusing on the 159 detected X-linked proteins, 45 proteins (38%) were
401 significantly upregulated in both $X^{Mus}Y$ and $X^{Cast}O^{Mus}$ cells, indicating that some but not all
402 expressed proteins are compensated by XCU (**Figure 6b-c, Supplementary Fig. 9c-d,**
403 **Supplementary Table 3**). Compared to autosomes, the proportion of upregulated proteins
404 was highly enriched on the X chromosome (**Figure 6d**). At the protein level, upregulated X-
405 linked proteins were enriched for proteins that are part of complexes, suggesting evolution
406 selected dosage compensation mechanisms for these proteins (**Figure 6e**). Taken together,
407 our data suggest that a subset of X-linked genes are compensated by XCU at the protein
408 level in $X^{Mus}Y$ and $X^{Cast}O^{Mus}$ mESCs.

To determine if the same genes are compensated at the RNA and protein level, we integrated the proteomics and transcriptomics data and compared genes only present in both RNA and protein data. We found that of the 159 coding genes covered in both datasets, a majority, 103 (60%), were more abundant in XO samples compared to the copy-number corrected abundance in XX (**Figure 6f**). Specifically, 47 (28%) showed both increased RNA and protein levels, whereas 56 (35%) genes were increased at the protein level only, suggesting exclusive post-transcriptional dosage compensation of these genes. A small proportion of genes were increased at the RNA level only (8%), while 27% of genes did not show compensation at the RNA or protein level. Despite the limited sensitivity of proteomics compared to transcriptomics and the commonly reported RNA-protein discordance[63], we observed a positive correlation in upregulation (r=0.37). These results indicate that the contribution of RNA and protein regulation to dosage compensation by XCU may vary for different X-linked genes in mESCs, in agreement with transcription and protein measurements in the brain[62]. Our results reveal that there are multiple layers of gene and protein regulation involved in dosage compensation by XCU of individual X-linked genes in ESCs.

Next, we examined dosage compensation at the protein level in two heterozygous segmental deletion lines E and K. To assess XCU, we analyzed protein abundance normalized to copy number, based on information on genetic regions with one or two copies. Outside the deleted regions, there was no XCU at the protein level (**Figure 6g**, **Supplementary Fig. 9e**). In contrast, within the deleted regions, we detected considerable XCU at the protein level (**Figure 6h**, **Supplementary Fig. 9f**). The upregulation status of individual proteins that are upregulated in $X^{Mus}Y$ and $X^{Cast}O^{Mus}$ lines was evaluated in the deleted ESC lines (**Figure 6i**). Proteins encoded outside the deleted regions remained unchanged, while several proteins within deleted regions were upregulated. In summary, our results reveal the existence of different dosage compensation mechanisms in mouse PSCs, with genes that tend to be compensated at the protein, RNA or both levels, and to varying degrees. Together, we conclude that ESCs can compensate for mono-allelic gene expression by XCU at both RNA and protein levels.

DISCUSSION

In this study, we investigated dosage compensation and sensing in PSCs. We discovered that dosage of monosomically expressed X-linked and autosomal regions is compensated at both the mRNA and protein levels. In addition, we found that dosage compensation does not require one or more specific regions on the X chromosome involved in dosage sensing and XCU. In contrast, our findings indicate that XCU is regulated at a gene-by-gene level and involves upregulation of expression at the transcriptional and protein levels.

These results support previous findings by others and us related to elastic tuning of dosage compensation with one allele becoming upregulated upon inactivation or loss of the other allele during development[16,20]. In addition, our studies are in line with reports showing that XCU is not global, as not all X-linked genes are transcriptionally upregulated[17]. Our data do indicate that a majority of proteins detected by mass spectrometry display XCU at the

protein level. This finding may involve an over-interpretation of the percentage of genes subject to XCU as our findings indicate that XCU genes are expressed at a higher level and will therefore be more easily detected. On the contrary, our study only examined PSCs and different cell types or cell states may require dosage compensation of different genes[17,62,64]. We conclude that the mammalian genome is more adaptive and robust than previously suggested.

Our studies and others also indicate that different dosage compensation mechanisms or different combinations of mechanisms are in place to regulate gene dosage compensation. These mechanisms include transcriptional burst and translation initiation frequency as well as mRNA and protein stability[19,26,62]. We hypothesize that self-regulating feedback loops and enhancers may play a role in sensing changes in gene dosage, as inactivation or deletion of one allele could drive differential transcription factor binding *in trans*. This could then also be related to the increased transcriptional burst frequency which has been reported with XCU[16,19,20]. Furthermore, in line with the increased transcriptional burst frequency reported, we found an increased enrichment of one histone modification, H4K9ac, associated with active transcription at the transcription start sites of genes subject to XCU. These results show that H4K9ac is associated with XCU, however, whether this mark is instructive or sufficient to induce dosage compensation remains to be tested. Notably, H4K16ac was not significantly enriched indicating that mammalian cells employ distinct mechanisms compared to *Drosophila* to upregulate expression of X-linked genes. As our study indicates that XCU is regulated on a gene-by-gene basis, identification of the mechanisms employed and interactions involved to regulate XCU requires further investigation at the gene level.

Studies in humans and primates have suggested that XCU also occurs in cells with a single active X chromosome[27,28,35,62]. We hypothesize that the gene-specific dosage sensing and subsequent compensation observed in mouse cells also occurs in human stem cells and in development. Furthermore, it has been suggested that XCU is widespread in placental mammals[4], so we would expect gene-specific dosage compensation to occur for many genes on the human X chromosome, however additional studies would be required to confirm this. Widespread dosage compensation of X-linked genes could explain why monosomy of the X chromosome (Turner syndrome) is the only viable monosomy in humans and mice[65,66]. Studying X-linked dosage compensation in early human development is difficult without allele-resolution data, and due to the low coverage of SNPs between human alleles, allele-resolution data is typically only available for a few genes.

Our findings have implications for human disorders caused by haploinsufficiency. First, dosage compensation of autosomes may have evolved to cope with heterozygous mutations, monoallelic silencing, microdeletions or aneuploidies and their own effects. Second, dosage compensation may enable survival, but is not sufficient for restoring a wildtype phenotype and rescuing haploinsufficiency and as such may enable diseased states.

Consistent with previous research in both human cancers and embryos, our findings provide strong evidence for dosage compensation of autosomal genes[3,67]. This suggests that the mammalian genome possesses an inherent ability to compensate for gene dosage imbalances resulting from genomic loss or decreased expression, a capacity that extends beyond the X chromosome. This intrinsic dosage compensation mechanism may have been a key factor in the evolution of X-chromosome inactivation (XCI). As X-linked genes were progressively lost from the Y chromosome during the evolution of mammalian sex chromosomes[68], it is hypothesized that increasing selective pressure drove the development of dosage compensation mechanisms for X-linked genes. This likely led to the gradual incorporation of X-linked genes into the XCI process[8,34,69]. The gradual nature of this evolution may explain the gene-by-gene regulation observed in XCU.

In conclusion, our study supports the hypothesis of gene-by-gene regulation of X-linked gene dosage compensation involving multiple levels of regulation in a locus-specific manner to sense and compensate for variations in X-linked gene dosage.

METHODS

Generation of cell lines

XX female polymorphic mESCs (129/Sv-Cast/EiJ) with heterozygous deletions located between *Tfe3* and *Zic3*, *Zic3* and *Dusp9*, as well as between *Dusp9* and *Nr0b1* were obtained from Song et al., 2019[41]. XO mouse iPSCs used in scRNA-seq were generated by passaging XX-GFP female mouse iPSCs (129/Sv-Cast/EiJ, obtained from Talon et al., 2021[16]) to passage 14 before FACS for GFP negative cells (XO iPSCs) and collection for single-cell RNA-sequencing (see below). XX female iPSCs (129/Sv-Cast/EiJ) were derived as described in Talon at al., 2021[16]. XY male mESCs (C57BL/6J-Cast/EiJ) were obtained from Chen et al., 2016[70]. Both ESC and iPSC lines were used in this study, due to availability and experimental design constraints, however, evidence indicates that mouse iPSCs and ESCs behave equivalently with respect to X chromosome sensing and XCU[16,20].

For all newly generated lines, gRNAs (**Supplementary Table 4**) were integrated in the pSpCas9(BB)-2A-Puro V2.0 PX459 vector (Addgene #62988), enabling transient puromycin selection. Complementary oligonucleotides containing the gRNA sequence and compatible *BbsI* overhangs were annealed and ligated in PX459. To generate homology arm vectors, ~500–1000 bp 5′ and 3′ homology arms were amplified by overhang PCR from mouse genomic DNA with compatible restriction enzyme sequences. PCR products were purified from gel using the QIAquick® Gel Extraction Kit (Qiagen, 28506). Homology arm PCR products were digested with the indicated restriction enzymes and subsequently purified and ligated into compatible sites in the pCR™2.1-TOPO™ vector (Invitrogen, K450002). A neomycin resistance cassette flanked by LoxP sites was integrated in-between the 5’ and 3’ homology arms in an EcoRI restriction site for generating large X-chromosomal deletions. The cassette was retained in all deletion lines, as Cre-mediated excision was not required for downstream experiments.

532 Two independent *Rnf12*$^{+/-}$ cell lines were generated in F1 2–1 hybrid (129/Sv-Cast/Ei)
533 mESCs. Although the heterozygous *Rnf12* mutation was not essential for the deletion
534 experiments described here, it induces complete skewing upon XCI, which was relevant for
535 a parallel study. The first *Rnf12*$^{+/-}$ cell line was generated by introducing PX459 vectors
536 containing gRNAs targeting intron 2 and the 3'UTR. This *Rnf12*$^{+/-}$ cell line served as the
537 parental cell line for generating deletions A through I and K, as well as the *Rnf12*$^{+/-}$*Pdzd4*$^{+/-}$
538 lines. Attempts to induce deletion J in this line failed due to chromosomal instability and
539 subsequent X chromosome loss. Therefore, a second *Rnf12*$^{+/-}$ cell line was generated by
540 introducing PX459 vectors with alternative gRNAs. This line served as the parental
541 background for del J and I-TEL.

542 The first *Rnf12*$^{+/-}$ was generated by transfecting gRNAs by electroporation in Gene Pulser
543 0.2 cm-gap cuvettes (Biorad, 1652086) at 118 kV, 1200 μF and ∞Ω in a Gene Pulser xCell
544 electroporation system (Biorad). 24h post-transfection, the medium was refreshed and
545 supplemented with 1 μg mL−1 puromycin (Sigma-Aldrich, P8833) for 36h. Drug-resistant
546 clones were characterized by PCR spanning the deletion. All other cell lines were generated
547 by transfecting the plasmids with Lipofectamine 2000 (Invitrogen, 11668019) in 6 × 10^5
548 mESCs dissociated into single-cells. Each transfection contained 2 μg of the homology arm
549 vector and 1 μg of PX459 containing gRNAs targeting the 5' or 3' end of the deletion. 24h
550 post-transfection, the medium was refreshed and supplemented with 1 μg mL−1 puromycin
551 for 48h followed by refreshing with medium supplemented with 285 μg mL−1 Geneticin
552 (G418)(Gibco, 11811-031) for 4-6 days. No Geneticin/neomycin selection was performed for
553 generating the *Rnf12*$^{+/-}$ and the *Rnf12*$^{+/-}$*Pdzd4*$^{+/-}$ cell lines. Drug-resistant clones were
554 characterized by PCR targeting genotype-specific length polymorphisms inside and outside
555 the targeted deletion (**Supplementary Table 5**). CRISPR-Cas9 targeting of X-linked regions
556 results in a population of cells losing part of the X chromosome extending beyond the
557 targeted regions. These deletion clones were identified and characterized by PCR (Del AB,
558 C-G and I-TEL). Deletion clones were identified and characterized by PCR and the deletion
559 boundaries were determined using allele-specific RNA sequencing data. Another population
560 of cells lost the entirety of one of the X chromosomes. These XO mESC lines were included
561 in the bulk RNA-seq analysis as treatment-matched XO controls.

562

563 **Cell culture**

564 Mouse embryonic fibroblasts (MEFs) were cultured in MEF medium [DMEM (Gibco, 10829-
565 018) supplemented with 10% (v/v) fetal bovine serum (FBS, Gibco, 10500-064), 1% (v/v)
566 penicillin/streptomycin (P/S, Gibco, 15140122), 1% (v/v) Glutamax (Gibco, 35050038), 1%
567 (v/v) non-essential amino acids (NEAA, Gibco, 11140035), and 0.008% (v/v) beta-
568 mercaptoethanol (Gibco, 31350010)]. Mouse iPSCs and mESCs were grown on Mitomycin-
569 treated MEFs in mESC medium [KnockOut DMEM (Gibco, 10829-018) supplemented with

570 15% FBS (Gibco, 10500-064), 1% (v/v) penicillin/streptomycin (P/S, Gibco, 15140122), 1%
571 (v/v) Glutamax (Gibco, 35050038), 1% (v/v) non-essential amino acids (NEAA, Gibco,
572 11140035), 0.008% (v/v) beta-mercaptoethanol (Gibco, 31350010), and mouse LIF
573 (1000U/mL, home-made) at 37°C under 5% CO2. *Rnf12+/-*, deletion lines A to K and
574 matched controls were grown on irradiated MEFs in adjusted mESC medium [DMEM
575 (Gibco, 11995065), 15% FBS (Capricorn Scientific, FBS-12A), 1% (v/v)
576 penicillin/streptomycin (Sigma-Aldrich, P0781), 1% (v/v) NEAA (Lonza, BE13-114E),
577 0.1 mM beta-mercaptoethanol and LIF (5000 U/ml, home-made)]. mESCs and iPSCs were
578 passaged every two days using trypsin dissociation.

579

580 **Cell sorting**

581 Cells were dissociated using trypsin digestion and subsequently washed in incubation
582 buffer (1x PBS, 0.5% BSA, 2mM EDTA) and filtered through a Falcon 40um Cell Strainer
583 (Corning, 352340). 1µg SSEA1-PE antibody (R&D Systems, FAB2155P) was added per 5
584 million cells. Cells were incubated for 30 min at 4°C. Cell death exclusion was performed by
585 adding DAPI (Sigma-Aldrich, D9542) prior to sorting. Sorting was performed on a BD
586 FACSAria Fusion (BD Biosciences) and performed by expert operators at the VIB FACS
587 core.

588

589 **Single-cell RNA-seq library preparation**

590 Single-cell RNA-seq libraries were prepared by following a previously published protocol
591 (Smartseq3xpress)[44], with minor modifications. Library quality was checked using an Agilent
592 Tapestation as well as an Agilent 2100 Bioanalyzer. Library concentration was checked with
593 a Qubit fluorometer (Qubit dsDNA HS Assay).

594

595 **Single-cell RNA-seq sequencing**

596 Single-cell RNA-seq libraries were sequenced in paired-end mode (150bp) by BGI
597 Genomics (Shenzhen, China) on a DNBSEQ-G400 sequencer (MGI Tech).

598

599 **Single-cell RNA-seq analysis**

600 Single-cell RNA-seq data was obtained as fastq files from BGI Genomics. The zUMIs[71]
601 pipeline was used to map reads using STAR[72] (v2.7.1a) with the options '--
602 clip3pAdapterSeq CTGTCTCTTATACACATCT'. Reads containing barcodes which
603 corresponded to XX, XO, Deletion 1, Deletion 2, or Deletion 3 cells were mapped to an
604 GRC38.p6 mouse reference genome N-masked for SNPs between the 129/SvJ and Cast
605 strains and SNPs between Bl6 and 129. Reads containing barcodes which corresponded to
606 XY cells were mapped to an GRC38.p6 mouse reference genome N-masked for SNPs
607 between the Bl6 and Cast strains. Reads were filtered such that reads containing at least 3
608 bases with Phred quality score less than 20 were omitted. Allele-resolution counts were
609 generated using a publicly available script 'get_variant_overlap_CAST.R'
610 (https://github.com/sandberg-lab/Smart-seq3/)[73] and a custom list of SNPs between

611 129/SvJ and Cast, with overlapping SNPs between 129/SvJ and Bl6, as well as overlapping
612 SNPs between Cast and Bl6 omitted. Allelic exon UMI counts were used to generate Seurat
613 [74] (v4.2.1) objects, which were then filtered such that cells with less than 10,000 UMIs for
614 either allele were omitted. After filtering, we obtained 69 $X^{Cast}X^{Mus}$, 44 $X^{Cast}O^{Mus}$, 6 $X^{Mus}O^{Cast}$,
615 61 $X^{Mus}Y$, 52 Deletion 1, 51 Deletion 2, and 41 Deletion 3 cells. Read counts were
616 normalized to TPM (transcripts per million). Normalized allele resolution UMI counts were
617 used for all analysis on the scRNA-seq dataset. Mean normalized gene expression was
618 calculated for genes between the 10th and 90th percentile of expression per cell for each
619 gene set of interest (all X-linked genes, inside/outside each deletion, inside/outside
620 inactivated region), and for all (other) autosomal genes. X-to-autosome ratio was calculated
621 by dividing the mean expression of genes in each subset by the median expression of
622 autosomal genes.

623

624 **Characterization of X-chromosome status**

625 The mean expression of X-linked genes from each allele was considered for each cell. If the
626 mean allelic expression was greater than two for the *Cast* allele and less than two for the
627 *Mus* allele, then the cell was defined as $X^{Cast}O^{Mus}$, and vice versa. One cell was omitted due
628 to ambiguous X-status.

629

630 **Characterization of pluripotency status**

631 The pluripotency marker genes *Essrb*, *Nanog*, and *Pou5f1* were used to assess
632 pluripotency status. High expression levels ($\log_2$(TPM) > 2.5) of each marker gene was
633 considered to be sufficient to conclude the cells had not differentiated and remained
634 pluripotent.

635

636 **Identification of XCU genes**

637 The expression values of each X-linked genes from the active allele of cells with a single
638 active X chromosome (X^{Cast} expression from $X^{Cast}O^{Mus}$, X^{Mus} expression from $X^{Mus}O^{Cast}$ and
639 $X^{Mus}Y$) was tested to be greater than half of the total allelic expression from XX cells via
640 Student's T.test. Genes with $p<0.05$ and fold change > 1.2 were defined as being
641 transcriptionally upregulated.

642

643 **Characteristics of XCU genes**

644 A list of known escapee genes was downloaded from Berletch *et al.* 2015[56] and overlapped
645 with the list of upregulated genes in $X^{monosomy}$ and non-upregulated genes. The EMBL-EBI
646 protein complex database[75] was used to compare the proportion of genes which code for
647 proteins in complexes between upregulated and non-upregulated genes. The CD-CODE
648 database was used to determine the proportion of transcriptionally upregulated X-linked
649 genes which code for proteins that form condensates[76]. Human orthologs of upregulated X-
650 linked genes were identified using the BioMart tool from Ensembl[77]. This list of orthologs
651 was then overlapped with a list of known disease causing genes from the OMIM

database[78]. Significant differences between the lists of genes were calculated using a Student's t-test when comparing expression and a Chi-square test when comparing proportions.

The lists of upregulated and non-upregulated genes were examined for gene ontology (GO) biological processes (BP) and protein-protein interaction (PPI) enrichment using Enrichr[79]. Significant terms (p-value < 0.05) were selected for each database and gene list, and the top 10 terms for each category were visualized in barplots.

Bulk RNA-seq

Cells were cultured at least two passages before harvesting. mESCs were depleted of MEFs by pre-plating dissociated cells for 45 minutes at 37°C in non-gelatinized plates. The supernatant containing mESCs was spun down for 5 min at 300 × g. Cell pellets were lysed and RNA was extracted using the ReliaPrep™ RNA Miniprep kit (Promega, Z6012) with increased DNase treatment (25 min at room temperature). MEF depletion was validated on the genomic DNA of part of the cell pellet using PCRs targeting genotype-specific length polymorphisms and SNPs.

Sequencing libraries were prepared using the Truseq stranded mRNA library preparation method from Illumina. The libraries of the XO cells were subsequently sequenced on an Illumina NextSeq2000 sequencer resulting in single read clusters of 50 bases in length. The libraries of all other cell lines were sequenced on a HiSeq2500 sequencer resulting in paired-end clusters of 50 bases.

Bulk RNA-seq analysis

The SNPs in the 129/Sv and Cast/Ei lines were downloaded from the Sanger Institute (v.5 SNP142)[80]. These were used as input for SNPsplit[81] (v0.3.4), to construct an N-masked reference genome based on mm10 in which all SNPs between 129/Sv and Cast/Ei are masked. The reads were trimmed and aligned to the N-masked reference genome using TrimGalore[82] (v0.6.7) and HISAT2[83] (v2.2.1), respectively. SNPsplit was then used to assign the reads to either the 129/Sv or Cast/Ei BAM file based on the best alignment or to an unassigned BAM file if mapping to a region without allele-specific SNPs (--paired for the paired-end samples). The allele-specific and unassigned BAM files were merged into a composite BAM file using Samtools[84] (v1.10). The number of mapped reads per gene was counted for both alleles separately and for the composite BAM file using featureCounts[85] (v2.0.6) based on the gene annotation from Ensembl v98 (-t exon -s 2). The raw counts were normalized to transcripts per million (TPM).

Validation of bulk RNA-seq samples

All bulk RNA-seq samples were generated in a *Rnf12*$^{+/-}$ parental cell line. To assess a potential bias, we performed differential expression analysis between WT XX and *Rnf12*$^{+/-}$ XX mESCs using DESeq2[86] (v1.30.1) with default settings. Results were plotted in a scatter plot showing mean TPM in both cell lines, in which all differential expressed genes

(adjusted p-value < 0.05, $\log_2$(fold change) < -1 or > 1) are highlighted. The deleted regions in all samples were validated by calculating the ratio of each sample to the mean of the parental *Rnf12*$^{+/-}$ samples. One deletion A clone and both deletion G clones were excluded due to a suspected recombination event rather than deletion. To ensure comparability across the remaining samples, we assessed the expression levels of the pluripotency genes *Essrb*, *Nanog* and *Pou5f1* by plotting their TPM values for all samples. Additionally, global expression patterns were evaluated by calculating the Pearson correlation coefficients for TPMs of all autosomal genes, which were visualized in a heatmap.

XCU in bulk RNA-seq data

To maximize statistical power, we analyzed non-allelic TPMs of all X-linked genes within and outside each deletion region. Only expressed genes were selected by filtering for TPM > 5 in *Rnf12*$^{+/-}$ samples. Deletion I was excluded from the plots showing expression within each deletion region due to insufficient expressed genes. For each genomic region, mean TPM values were calculated. These levels were compared to the mean XX level (from *Rnf12*$^{+/-}$) and 50% of the mean XX level, representing the expected expression level for a single X chromosome without upregulation.

To account for copy number differences, gene expression was normalized to copy number-corrected values by dividing TPM values by the number of copies present, based on the genomic locations of each deletion. Mean copy number-corrected TPMs were then calculated for genes within and outside deletion regions and compared to the mean copy number-corrected TPM in XX samples.

To validate allelic upregulation detected in non-allelic TPM values, we selected X-linked genes with a fold change > 1.2 in copy number-corrected TPMs between XO and XX cells. For this subset of upregulated genes, allelic *Cast* expression data was filtered, and the $\log_2$ fold change between XO and XX cells was calculated. The allelic upregulation status in XO cells for each gene, annotated by overlapping deletion region, was visualized in a heatmap. The level of upregulation in the deletion samples was assessed by analyzing the copy number-corrected expression of genes upregulated in XO cells. For each gene, the $\log_2$ fold change relative to the mean expression in XX cells was calculated. These values were plotted separately for genes located inside and outside each deletion, with median values per sample indicated. For visualization, extreme values were clipped at -1 and 4. Statistical significance was assessed using two-sided paired t-tests on the mean expression per genotype, with Bonferroni correction for multiple comparisons. No statistical testing was performed for genes located within the deletions due to the limited number of genes per deletion region.

Autosomal upregulation analysis

We reanalyzed a bulk RNA-seq dataset from GSE119602 using the same approach as described in 'Bulk RNA-seq analysis'. Inactive genes were defined as genes whose fold change was less than 0.15 when comparing samples with doxycycline to samples without

734 doxycycline. The inactive region was defined as the region from 80Mb to the 3' telomere.
735 Upregulated genes were defined as genes with a fold change greater than 0.5 when
736 comparing samples with doxycycline to samples without doxycycline. Characteristics of the
737 upregulated genes were evaluated as described in 'Characteristics of XCU genes'. Mean
738 normalized gene expression within/outside the inactive region for each allele was calculated
739 using genes with expression between the 5th and 95th percentile for each sample.

740

741 **RT-qPCR**

742 mESCs were pre-plated as described. Cell pellets were lysed and RNA was extracted using
743 the ReliaPrep™ RNA Miniprep kit (Promega, Z6012) with increased DNase treatment (25
744 min at room temperature). 500 ng RNA was reverse transcribed using Superscript III
745 (Invitrogen, 18080093) and random hexamers (Invitrogen, N8080127) with the addition of
746 RNaseOUT (Invitrogen, 10777019). cDNAs were diluted 1:1 in water. RT-qPCRs were
747 performed in triplicate in the GoTaq qPCR Master Mix (Promega, A6002) in a CFX384
748 Touch Real-Time PCR Detection System (BioRad, LJB22YE8Z). *Rplp0* and *H2afz* were
749 used as normalization controls. Allele-specific primer pairs were optimized using pure
750 gDNA of 129/Sv and Cast/Ei mice. All primers are included in (**Supplementary Table 6**).

751

752 **Proteomics**

753 Proteomics experiments were performed on $X^{Cast}X^{Mus}$ (*Rnf12*$^{+/-}$), $X^{Mus}Y$ (F1 2-3), and $X^{Cast}O^{Mus}$
754 (*Rnf12*$^{+}$) ESCs. Additionally, two deletion cell lines (Deletion E and K in *Rnf12*$^{+/-}$) were
755 included, selected based on their single-region deletions and a high proportion of
756 transcriptionally upregulated genes.

757 For global proteome analysis of whole cell extracts, cells were lysed in 100 mM Tris/HCl,
758 pH 8.2, containing 1 % sodium deoxycholate (SDC) using sonication in a Bioruptor Pico
759 (Diagenode). Protein concentrations were measured using the BCA assay (ThermoFisher
760 Scientific). 100 µg protein was reduced in lysis buffer with 5 mM dithiothreitol and alkylated
761 with 10 mM iodoacetamide. Next, proteins were digested with 2.5 µg trypsin (1:40
762 enzyme:substrate ratio) overnight at 37 °C. After digestion, peptides were acidified with
763 trifluoroacetic acid (TFA) to a final concentration of 0.5 % and centrifuged at 10,000 g for 10
764 min to spin down the precipitated SDC. Peptides in the supernatant were desalted on a 50
765 mg C18 Sep-Pak Vac cartridge (Waters). After washing the cartridge with 0.1 % TFA,
766 peptides were eluted with 50 % acetonitrile and dried in a Speedvac centrifuge. Peptides
767 were then analyzed by nanoflow LC-MS/MS as described below.

768 Nanoflow LC-MS/MS was performed on an Vanquish Neo LC system coupled to an
769 Orbitrap Exploris 480 mass spectrometer (both ThermoFisher Scientific), operating in
770 positive mode and equipped with a nanospray source. Peptide mixtures were trapped on a
771 PepMap trapping column (2 cm × 100 µm, Thermo, 164750) at a flow rate of 1 µl/min.
772 Peptide separation was performed on ReproSil C18 reversed phase column (Dr Maisch
773 GmbH; column dimensions 25 cm × 75 µm, packed in-house) using a linear gradient from 0
774 to 80% B (A = 0.1% FA; B = 80% (v/v) AcN, 0.1 % FA) in 120 min and at a constant flow

775 rate of 250 nl/min. The column eluent was directly sprayed into the ESI source of the mass
776 spectrometer.

777 For data independent acquisition (DIA), all spectra were recorded at a resolution of 120,000
778 for full scans in the scan range from 350–1100 m/z. The maximum injection time was set to
779 50 ms (AGC target: 4E5). For MS2 acquisition, the mass range was set to 336–1391 m/z
780 with variable isolation windows ranging from 7–82 m/z with a window overlap of 1 m/z. The
781 orbitrap resolution for MS2 scans was set to 30,000. The maximum injection time was at 54
782 ms (AGC target: 5E4; normalized AGC target: 100 %).

783

784 **Proteomics analysis**

785 DIA raw data files were analyzed with the Spectronaut Pulsar X software package (version
786 17.0.221202, www.biognosys.com), using directDIA for DIA analysis including MaxLFQ as
787 the LFQ method and Spectronaut's IDPicker algorithm for protein inference. The Q-value
788 cutoff at precursor and protein level was set to 0.01. All imputation of missing values was
789 disabled.

790 Proteins detected at least once in each sample were retained for further analysis. The mean
791 abundance of all X-linked proteins in each XX, XO and XY sample was plotted with
792 confidence intervals using seaborn pointplot. To avoid a detection bias of low-abundance
793 proteins between X-linked (1n in XO and XY cells) and autosomal proteins (2n), X:A ratios
794 were calculated using only proteins with a mean abundance greater than 12,000,000 in the
795 XX samples (2n for all proteins). The X:A ratio was defined as the abundance of each X-
796 linked protein divided by the mean autosomal abundance in the same sample, and
797 visualized using seaborn pointplot.

798 Since proteomics data lacks allele-specific resolution, we corrected the data for the copy
799 number to identify significantly upregulated proteins. The abundances in XX samples were
800 divided by 2 to account for two alleles, while abundances of XO and XY samples remained
801 unchanged. Moreover, autosomal abundances were divided by 2 in all samples. Differential
802 expression analyses were performed between XO and XX and between XY and XX using a
803 Tuckey's HSD test. Upregulated proteins were selected based on the criteria of $\log_2$(fold
804 change) > 0 and p-value < 0.05 in both XY and XO comparisons. The results for all X-linked
805 proteins were visualized using volcano plots, and the number of upregulated proteins per
806 chromosome were displayed in a barplot. To assess the overlap in upregulation between
807 XO and XY cells, gene lists identified in each analysis were compared using a Venn
808 diagram. In addition, a scatter plot was generated to visualize the correlation between cell
809 lines, showing the $\log_2$ fold change in copy number-corrected abundances for XO vs XX
810 and XY vs XX. The correlation between transcriptomic and proteomic upregulation was
811 explored using a scatter plot showing the $\log_2$ fold change of the copy number-corrected
812 abundances in XO versus XX and the copy number-corrected transcript expression in XO
813 versus XX.

Samples with deletions E and K were analyzed by labeling proteins according to the genomic location of the gene encoding the protein (inside or outside the deleted region). For each region separately, the mean normalized protein abundance was plotted, comparing levels outside and inside the deletion to the XX reference level and 50% of the XX reference level, respectively. Abundances were copy number-corrected by halving abundances for two-copy proteins. These corrected abundances were visualized in a heatmap, focusing on proteins significantly upregulated in XO and XY samples.

ChIP-seq

mESCs were depleted of MEFs 16 hours before the harvest by pre-plating dissociated cells for 45 minutes at 37°C in non-gelatinized plates. In total, 1 × 10^8 cells were crosslinked by the addition of 1% formaldehyde (Sigma-Aldrich, F1635-25ML) to the dish and incubated at room temperature for 10 minutes on a rocking platform. Formaldehyde was quenched by adding 125 mM glycine for 5 minutes. Subsequently, cells were washed once with 1 × PBS before scraping in 1 × PBS supplemented with 1× protease inhibitors (Roche, 11836170001). Cells were pelleted, resuspended and incubated for 10 minutes at 4°C in 1 × LB1 (50 mM HEPES pH 8.0, 140 mM NaCL, 1mM EDTA, 10% glycerol, 0.5% NP-40, 0.25% Triton X-100, 1× protease inhibitors), in 1 × LB2 (10 mM Tris-HCl pH 8.0, 200 mM NaCl, 1 mM EDTA, 0.5 mM EGTA,1× protease inhibitors) and in 1× LB3 (10 mM Tris-HCl pH 8.0, 100 mM NaCl, 1 mM EDTA, 0.5 mM EGTA, 0.1% Sodium Deoxycholate, 0.5% N-laurolylsarcosine, 1× protease inhibitors). DNA was sonicated to an average fragment length of 100-300 bp using a Bioruptor Pico (Diagenode, B01060001) for 10 cycles of 30 sec on and 30 sec off. 1/20th volume of 20% Triton X-100 was added to the sonicated chromatin, and incubated for 10 minutes at 4°C before centrifugation for 10 min at 4500 × g 10 at 4°C to remove debris. 10 µl chromatin was used to measure the chromatin concentration by nanodrop and check the sonication efficiency. Sheared chromatin was flash frozen in liquid nitrogen and stored at -80°C until further use. For H4K16ac ChIPs, 30 µg of chromatin was diluted to 500 µl in ChIP dilution buffer (16.7 mM Tris-HCl pH 8.0, 167 mM NaCl, 1.2 mM EDTA, 1.1% Triton X-100, 0.01% SDS, 1× protease inhibitors) and incubated while rotating overnight at 4°C with 2 µg H4K16ac antibody (Sigma-Aldrich, 07-329, lot: 3772263) or IgG (Sigma-Aldrich, 12-370). 30 µl of Magnetic beads (Life Technologies, 10004D) were washed once in ChIP dilution buffer, added to each sample and incubated while rotating for 4 hours at 4°C. Beads were washed 3× in Low salt buffer (20 mM Tris-HCl pH 8.0, 150 mM NaCl, 2 mM EDTA, 1% Triton X-100, 0.1% SDS, 1× protease inhibitors), 1× in High salt buffer (20 mM Tris-HCl pH 8.0, 500 mM NaCl, 2 mM EDTA, 1% Triton X-100, 0.1% SDS, 1× protease inhibitors), 1× in LiCl buffer (10 mM Tris-HCl pH 8.0, 250 mM LiCl, 1 mM EDTA, 1% NP-40, 1% Sodium Deoxycholate, 1× protease inhibitors) and rinsed once in TE (10 mM Tris-HCl pH 8.0, 1 mM EDTA), 10min rotating at 4°C each wash. Chromatin was eluted in 200µL Elution Buffer (1% SDS, 0.1M NaHCO3)

853 with 5µL protease K (10mgmL−1) and 2µL RNAse A (10mgmL−1) while shaking at
854 1,000rpm on an orbital thermal-mixer for 2h at 37°C followed by 65°C overnight. DNA was
855 purified using the Zymo ChIP DNA clean concentrator kit (Zymo Research, D5202)
856 according to the manufacturer's instructions and eluted in 15µL H2O. 0.1 µL DNA was used
857 per qPCR to validate ChIP enrichment.

858 The ChIP-seq libraries were prepared with the ChIPThruPLEX method (Takara Bio,
859 R400675). These libraries were subsequently sequenced on an Illumina NextSeq2000
860 sequencer. Paired-end clusters were generated of 50 bases in length.
861
862 **ChIP-seq analysis**
863 The ChIP-seq samples were analyzed allele-specifically similar to the bulk RNA-seq
864 analysis. The reads were trimmed using Trim Galore and mapped to the N-masked
865 reference genome using Bowtie2[87] (v2.5.0). Bam files were split by allele using SNPsplit and
866 the resulting allele-specific bam files were normalized to counts per ten million (CP10M)
867 using the bamCoverage tool (-bs 1 --normalizeUsing CPM) from deepTools[88] (v3.5.5).
868 Moreover, allele-specific tracks from GSE116480 were downloaded, including CP10M-
869 normalized data for H3K17me3, H3K27ac, H4ac, H2AK119Ub, H3K4me1, H3K4me3 and
870 H3K9ac after 0, 4, 12 and 24 hours of doxycycline.

871 Enrichment of all ChIP-seq tracks was plotted for each allele separately on the genomic
872 regions of upregulated and not upregulated genes, selected based on the scRNA-seq
873 analysis. Mean enrichment per bin was calculated using deepTools computeMatrix (scale-
874 regions -bs 100 --averageTypeBins mean --missingDataAsZero -m 3000 --upstream 1500 -
875 -downstream 1500). Profile plots were generated using custom Python (v3.9.16) scripts.
876 The matrix file from deepTools was loaded, and average enrichment profiles per bin were
877 plotted using seaborn line plot, including standard error bands.

878 To evaluate temporal patterns and assess statistical significance, we calculated the mean
879 signal in two genomic regions: (1) the promoter region, defined as 1 kb upstream of the TSS
880 to the TSS, and (2) the gene body, defined as the region spanning from TSS to TES. For
881 each region, bed files were generated containing the corresponding genomic coordinates
882 for all genes. These bed files were used as input for deepTools multiBigwigSummary, along
883 with all allele-specific bigwig files, to calculate the average scores in these regions.
884 Changes over time were visualized with line plots, showing the mean CP10M score with
885 standard errors for upregulated and not upregulated genes separately.

886 Statistical testing was performed for each gene set separately. Significant differences
887 between 0 and 24 hours were calculated using two-sided paired t-tests, with P-values
888 corrected for multiple testing with the Benjamini-Hochberg approach. These adjusted P-
889 values were added next to each gene set in the ChIP-seq line plots. Additionally,
890 differences between upregulated and not upregulated genes were tested using two-sided
891 Student's t-tests, also corrected for multiple testing. The resulting significance was added

above the corresponding regions in the profile plots.

Genome browser overviews were created to show ChIP-seq enrichment on the active upregulated allele at the loci of three upregulated genes. Tracks were selected based on significant differences in enrichment between 0 and 24 hours, as well as between upregulated and non-upregulated genes at 24 hours. CP10M-normalized allele-specific tracks for the significantly enriched marks were visualized using IGV v2.19.4[89].

Statistics and reproducibility

No statistical method was used to predetermine sample size. One cell was excluded from the scRNA-seq analysis due to ambiguous allelic expression from the X chromosome. One deletion A clone and both deletion G clones were excluded from RNA-seq analysis due to suspected recombination events or partial XO genotype, rather than the intended deletion.

DATA AVAILABILITY

The RNA-seq and ChIP-seq data generated in this study have been deposited in the NCBI Gene Expression Omnibus (GEO) database under accession code GSE282792 (https://www.ncbi.nlm.nih.gov/geo/query/acc.cgi?acc=GSE282792). Moreover, RNA-seq and ChIP-seq datasets from GSE119602 and GSE116480 were reanalyzed.
The mass spectrometry proteomics data have been deposited to the ProteomeXchange Consortium via the PRIDE partner repository with the dataset identifier PXD057399 (https://proteomecentral.proteomexchange.org/cgi/GetDataset?ID=PXD057399).
Source data are provided with this paper.

CODE AVAILABILITY

Code is available on the Pasque Lab GitHub account and can be accessed via the following link: https://github.com/pasquelab/Mice-XCU (ref.)

918 **REFERENCES**

919 1. Maloy, S. Diploidy. in *Brenner's Encyclopedia of Genetics* 322–323 (Elsevier, 2013).
920 2. Storchova, Z. *Aneuploidy in Health and Disease*. (BoD – Books on Demand, 2012).
921 3. De Rossi, S. & Bianchi, F. *Aneuploidy: Etiology, Disorders, and Risk Factors*. (Nova
922 Science Publishers, 2012).
923 4. Cecalev, D., Viçoso, B. & Galupa, R. Compensation of gene dosage on the mammalian
924 X. *Development* **151**, (2024).
925 5. Disteche, C. M. Dosage compensation of the sex chromosomes and autosomes.
926 *Semin. Cell Dev. Biol.* **56**, 9–18 (2016).
927 6. Brockdorff, N. & Turner, B. M. Dosage compensation in mammals. *Cold Spring Harb.*
928 *Perspect. Biol.* **7**, a019406 (2015).
929 7. Gu, L. & Walters, J. R. Evolution of Sex Chromosome Dosage Compensation in
930 Animals: A Beautiful Theory, Undermined by Facts and Bedeviled by Details. *Genome*
931 *Biol. Evol.* **9**, 2461–2476 (2017).
932 8. Gribnau, J. & Grootegoed, J. A. Origin and evolution of X chromosome inactivation.
933 *Curr. Opin. Cell Biol.* **24**, 397–404 (2012).
934 9. Ohno, S. *Sex Chromosomes and Sex-Linked Genes*. (Springer Verlag, 1967).
935 10. Graves, J. A., Disteche, C. M. & Toder, R. Gene dosage in the evolution and function of
936 mammalian sex chromosomes. *Cytogenet. Cell Genet.* **80**, 94–103 (1998).
937 11. Beukeboom, L. W. & Perrin, N. *The Evolution of Sex Determination*. (Oxford University
938 Press, USA, 2014).
939 12. Mattimoe, T. & Payer, B. The compleX balancing act of controlling X-chromosome
940 dosage and how it impacts mammalian germline development. *Biochem. J* **480**, 521–
941 537 (2023).
942 13. Lyon, M. F. Gene action in the X-chromosome of the mouse (Mus musculus L.). *Nature*
943 **190**, 372–373 (1961).
944 14. Brockdorff, N. *et al.* Conservation of position and exclusive expression of mouse Xist
945 from the inactive X chromosome. *Nature* **351**, 329–331 (1991).
946 15. Penny, G. D., Kay, G. F., Sheardown, S. A., Rastan, S. & Brockdorff, N. Requirement
947 for Xist in X chromosome inactivation. *Nature* **379**, 131–137 (1996).
948 16. Talon, I. *et al.* Enhanced chromatin accessibility contributes to X chromosome dosage
949 compensation in mammals. *Genome Biol* **22**, 302 (2021).
950 17. Naik, H. C., Hari, K., Chandel, D., Jolly, M. K. & Gayen, S. Single-cell analysis reveals X
951 upregulation is not global in pre-gastrulation embryos. *iScience* **25**, 104465 (2022).
952 18. Naik, H. C. *et al.* Lineage-specific dynamics of erasure of X-upregulation during
953 inactive-X reactivation. *bioRxiv* 2020.12.23.424181 (2023)
954 doi:10.1101/2020.12.23.424181.
955 19. Larsson, A. J. M., Coucoravas, C., Sandberg, R. & Reinius, B. X-chromosome
956 upregulation is driven by increased burst frequency. *Nat. Struct. Mol. Biol.* **26**, 963–969
957 (2019).
958 20. Lentini, A. *et al.* Elastic dosage compensation by X-chromosome upregulation. *Nat*
959 *Commun* **13**, 1854 (2022).
960 21. Deng, X. *et al.* Evidence for compensatory upregulation of expressed X-linked genes in

961 mammals, Caenorhabditis elegans and Drosophila melanogaster. *Nat. Genet.* **43**,
962 1179–1185 (2011).
963 22. Lin, H. *et al.* Relative overexpression of X-linked genes in mouse embryonic stem cells
964 is consistent with Ohno's hypothesis. *Nat. Genet.* **43**, 1169–70; author reply 1171–2
965 (2011).
966 23. Li, X. *et al.* Dosage compensation in the process of inactivation/reactivation during
967 both germ cell development and early embryogenesis in mouse. *Sci. Rep.* **7**, 3729
968 (2017).
969 24. Sangrithi, M. N. *et al.* Non-Canonical and Sexually Dimorphic X Dosage Compensation
970 States in the Mouse and Human Germline. *Dev. Cell* **40**, 289–301.e3 (2017).
971 25. Yildirim, E., Sadreyev, R. I., Pinter, S. F. & Lee, J. T. X-chromosome hyperactivation in
972 mammals via nonlinear relationships between chromatin states and transcription. *Nat*
973 *Struct Mol Biol* **19**, 56–61 (2011).
974 26. Rücklé, C. *et al.* RNA stability controlled by mA methylation contributes to X-to-
975 autosome dosage compensation in mammals. *Nat. Struct. Mol. Biol.* **30**, 1207–1215
976 (2023).
977 27. Okamoto, I. *et al.* The X chromosome dosage compensation program during the
978 development of cynomolgus monkeys. *Science* **374**, eabd8887 (2021).
979 28. Okamoto, I. *et al.* Eutherian mammals use diverse strategies to initiate X-chromosome
980 inactivation during development. *Nature* **472**, 370–374 (2011).
981 29. Deng, X. *et al.* Mammalian X upregulation is associated with enhanced transcription
982 initiation, RNA half-life, and MOF-mediated H4K16 acetylation. *Dev. Cell* **25**, 55–68
983 (2013).
984 30. Gupta, V. *et al.* Global analysis of X-chromosome dosage compensation. *J. Biol.* **5**, 3
985 (2006).
986 31. Lin, H. *et al.* Dosage compensation in the mouse balances up-regulation and silencing
987 of X-linked genes. *PLoS Biol.* **5**, e326 (2007).
988 32. Johnston, C. M. *et al.* Large-scale population study of human cell lines indicates that
989 dosage compensation is virtually complete. *PLoS Genet.* **4**, e9 (2008).
990 33. Moreira de Mello, J. C., Fernandes, G. R., Vibranovski, M. D. & Pereira, L. V. Early X
991 chromosome inactivation during human preimplantation development revealed by
992 single-cell RNA-sequencing. *Sci. Rep.* **7**, 10794 (2017).
993 34. Nguyen, D. K. & Disteche, C. M. Dosage compensation of the active X chromosome in
994 mammals. *Nat. Genet.* **38**, 47–53 (2006).
995 35. Fernandez Gallardo, E. *et al.* A multi-omics genome-and-transcriptome single-cell atlas
996 of human preimplantation embryogenesis reveals the cellular and molecular impact of
997 chromosome instability. (2023) doi:10.1101/2023.03.08.530586.
998 36. Vanneste, E. *et al.* Chromosome instability is common in human cleavage-stage
999 embryos. *Nat. Med.* **15**, 577–583 (2009).
1000 37. Mantzouratou, A. & Delhanty, J. D. A. Aneuploidy in the human cleavage stage embryo.
1001 *Cytogenet. Genome Res.* **133**, 141–148 (2011).
1002 38. Kojima, S. & Cimini, D. Aneuploidy and gene expression: is there dosage
1003 compensation? *Epigenomics* **11**, 1827–1837 (2019).

1004 39. Bravo-Estupiñan, D. M. *et al.* Gene dosage compensation: Origins, criteria to identify
1005 compensated genes, and mechanisms including sensor loops as an emerging
1006 systems-level property in cancer. *Cancer Med.* **12**, 22130–22155 (2023).
1007 40. Schukken, K. M. & Sheltzer, J. M. Extensive protein dosage compensation in aneuploid
1008 human cancers. *Genome Res.* **32**, 1254–1270 (2022).
1009 41. Song, J. *et al.* X-Chromosome Dosage Modulates Multiple Molecular and Cellular
1010 Properties of Mouse Pluripotent Stem Cells Independently of Global DNA Methylation
1011 Levels. *Stem Cell Reports* **12**, 333–350 (2019).
1012 42. Schulz, E. G. *et al.* The two active X chromosomes in female ESCs block exit from the
1013 pluripotent state by modulating the ESC signaling network. *Cell Stem Cell* **14**, 203–216
1014 (2014).
1015 43. Choi, J. *et al.* DUSP9 Modulates DNA Hypomethylation in Female Mouse Pluripotent
1016 Stem Cells. *Cell Stem Cell* **20**, 706–719.e7 (2017).
1017 44. Hagemann-Jensen, M., Ziegenhain, C. & Sandberg, R. Scalable single-cell RNA
1018 sequencing from full transcripts with Smart-seq3xpress. *Nat Biotechnol* **40**, 1452–1457
1019 (2022).
1020 45. Keane, T. M. *et al.* Mouse genomic variation and its effect on phenotypes and gene
1021 regulation. *Nature* **477**, 289–294 (2011).
1022 46. Doran, A. G. *et al.* Deep genome sequencing and variation analysis of 13 inbred mouse
1023 strains defines candidate phenotypic alleles, private variation and homozygous
1024 truncating mutations. *Genome Biol* **17**, 167 (2016).
1025 47. Pasque, V. *et al.* X Chromosome Dosage Influences DNA Methylation Dynamics during
1026 Reprogramming to Mouse iPSCs. *Stem Cell Reports* **10**, 1537–1550 (2018).
1027 48. Zvetkova, I. *et al.* Global hypomethylation of the genome in XX embryonic stem cells.
1028 *Nat Genet* **37**, 1274–1279 (2005).
1029 49. Janiszewski, A. *et al.* Dynamic reversal of random X-Chromosome inactivation during
1030 iPSC reprogramming. *Genome Res.* **29**, 1659–1672 (2019).
1031 50. Bird, K. A., Pires, J. C., VanBuren, R., Xiong, Z. & Edger, P. P. Dosage-sensitivity
1032 shapes how genes transcriptionally respond to allopolyploidy and homoeologous
1033 exchange in resynthesized Brassica napus. *Genetics* **225**, (2023).
1034 51. Birchler, J. A. & Veitia, R. A. The gene balance hypothesis: implications for gene
1035 regulation, quantitative traits and evolution. *New Phytol.* **186**, 54–62 (2010).
1036 52. Xie, Z. *et al.* Gene Set Knowledge Discovery with Enrichr. *Curr Protoc* **1**, e90 (2021).
1037 53. Pessia, E., Makino, T., Bailly-Bechet, M., McLysaght, A. & Marais, G. A. B. Mammalian
1038 X chromosome inactivation evolved as a dosage-compensation mechanism for
1039 dosage-sensitive genes on the X chromosome. *Proc. Natl. Acad. Sci. U. S. A.* **109**,
1040 5346–5351 (2012).
1041 54. Yang, L. *et al.* Phase separation as a possible mechanism for dosage sensitivity.
1042 *Genome Biol.* **25**, 17 (2024).
1043 55. Stortz, M., Presman, D. M. & Levi, V. Transcriptional condensates: a blessing or a curse
1044 for gene regulation? *Commun Biol* **7**, 187 (2024).
1045 56. Berletch, J. B. *et al.* Identification of genes escaping X inactivation by allelic expression
1046 analysis in a novel hybrid mouse model. *Data Brief* **5**, 761–769 (2015).

1047 57. Żylicz, J. J. *et al.* The Implication of Early Chromatin Changes in X Chromosome
1048 Inactivation. *Cell* **176**, 182–197.e23 (2019).
1049 58. Gelbart, M. E., Larschan, E., Peng, S., Park, P. J. & Kuroda, M. I. Drosophila MSL
1050 complex globally acetylates H4K16 on the male X chromosome for dosage
1051 compensation. *Nat Struct Mol Biol* **16**, 825–832 (2009).
1052 59. Galupa, R. & Heard, E. X-Chromosome Inactivation: A Crossroads Between
1053 Chromosome Architecture and Gene Regulation. *Annu Rev Genet* **52**, 535–566 (2018).
1054 60. Dixon, J. R. *et al.* Topological domains in mammalian genomes identified by analysis of
1055 chromatin interactions. *Nature* **485**, 376–380 (2012).
1056 61. Nesterova, T. B. *et al.* Systematic allelic analysis defines the interplay of key pathways
1057 in X chromosome inactivation. *Nat. Commun.* **10**, 3129 (2019).
1058 62. Wang, Z.-Y. *et al.* Transcriptome and translatome co-evolution in mammals. *Nature*
1059 **588**, 642–647 (2020).
1060 63. Liu, Y., Beyer, A. & Aebersold, R. On the Dependency of Cellular Protein Levels on
1061 mRNA Abundance. *Cell* **165**, 535–550 (2016).
1062 64. Lyu, Q. *et al.* A small proportion of X-linked genes contribute to X chromosome
1063 upregulation in early embryos via BRD4-mediated transcriptional activation. *Curr. Biol.*
1064 **32**, 4397–4410.e5 (2022).
1065 65. Yang, S. Diagnostic and therapeutic considerations in Turner syndrome. *Ann Pediatr*
1066 *Endocrinol Metab* **22**, 226–230 (2017).
1067 66. Ashworth, A., Rastan, S., Lovell-Badge, R. & Kay, G. X-chromosome inactivation may
1068 explain the difference in viability of XO humans and mice. *Nature* **351**, 406–408 (1991).
1069 67. Tang, Y. A. *et al.* Efficiency of Xist-mediated silencing on autosomes is linked to
1070 chromosomal domain organisation. *Epigenetics Chromatin* **3**, 10 (2010).
1071 68. Graves, J. A. M. Sex chromosome specialization and degeneration in mammals. *Cell*
1072 **124**, 901–914 (2006).
1073 69. Charlesworth, B. The evolution of chromosomal sex determination and dosage
1074 compensation. *Curr. Biol.* **6**, 149–162 (1996).
1075 70. Chen, G. *et al.* Single-cell analyses of X Chromosome inactivation dynamics and
1076 pluripotency during differentiation. *Genome Res* **26**, 1342–1354 (2016).
1077 71. Parekh, S., Ziegenhain, C., Vieth, B., Enard, W. & Hellmann, I. zUMIs - A fast and
1078 flexible pipeline to process RNA sequencing data with UMIs. *Gigascience* **7**, (2018).
1079 72. Dobin, A. *et al.* STAR: ultrafast universal RNA-seq aligner. *Bioinformatics* **29**, 15–21
1080 (2013).
1081 73. Hagemann-Jensen, M. *et al.* Single-cell RNA counting at allele and isoform resolution
1082 using Smart-seq3. *Nat. Biotechnol.* **38**, 708–714 (2020).
1083 74. Hao, Y. *et al.* Integrated analysis of multimodal single-cell data. *Cell* **184**, 3573–
1084 3587.e29 (2021).
1085 75. Meldal, B. H. M. *et al.* Complex Portal 2018: extended content and enhanced
1086 visualization tools for macromolecular complexes. *Nucleic Acids Res.* **47**, D550–D558
1087 (2019).
1088 76. Rostam, N. *et al.* CD-CODE: crowdsourcing condensate database and encyclopedia.
1089 *Nat. Methods* **20**, 673–676 (2023).

1090 77. Dyer, S. C. *et al.* Ensembl 2025. *Nucleic Acids Res* **53**, D948–D957 (2025).
1091 78. McKusick, V. A. *Mendelian Inheritance in Man: A Catalog of Human Genes and Genetic*
1092 *Disorders*. (JHU Press, 1998).
1093 79. Chen, E. Y. *et al.* Enrichr: interactive and collaborative HTML5 gene list enrichment
1094 analysis tool. *BMC Bioinformatics* **14**, 128 (2013).
1095 80. Sherry, S. T. *et al.* dbSNP: the NCBI database of genetic variation. *Nucleic Acids Res.*
1096 **29**, 308–311 (2001).
1097 81. Krueger, F. & Andrews, S. R. SNPsplit: Allele-specific splitting of alignments between
1098 genomes with known SNP genotypes. *F1000Res.* **5**, 1479 (2016).
1099 82. Krueger, F., James, F., Ewels, P., Afyounian, E. & Schuster-Boeckler, B.
1100 *FelixKrueger/TrimGalore: v0.6.7 - DOI via Zenodo*. (Zenodo, 2021).
1101 doi:10.5281/ZENODO.5127899.
1102 83. Kim, D., Paggi, J. M., Park, C., Bennett, C. & Salzberg, S. L. Graph-based genome
1103 alignment and genotyping with HISAT2 and HISAT-genotype. *Nat. Biotechnol.* **37**, 907–
1104 915 (2019).
1105 84. Li, H. *et al.* The Sequence Alignment/Map format and SAMtools. *Bioinformatics* **25**,
1106 2078–2079 (2009).
1107 85. Liao, Y., Smyth, G. K. & Shi, W. featureCounts: an efficient general purpose program
1108 for assigning sequence reads to genomic features. *Bioinformatics* **30**, 923–930 (2014).
1109 86. Love, M. I., Huber, W. & Anders, S. Moderated estimation of fold change and
1110 dispersion for RNA-seq data with DESeq2. *Genome Biol* **15**, 550 (2014).
1111 87. Langmead, B. & Salzberg, S. L. Fast gapped-read alignment with Bowtie 2. *Nat.*
1112 *Methods* **9**, 357–359 (2012).
1113 88. Ramírez, F., Dündar, F., Diehl, S., Grüning, B. A. & Manke, T. deepTools: a flexible
1114 platform for exploring deep-sequencing data. *Nucleic Acids Res* **42**, W187–91 (2014).
1115 89. Robinson, J. T. *et al.* Integrative genomics viewer. *Nat Biotechnol* **29**, 24–26 (2011).
1116 90. ryan-allsop, Pasque lab. pasquelab/Mice-XCU: X-chromosome upregulation
1117 operates on a gene-by-gene basis at RNA and protein levels. *Zenodo*
1118 https://doi.org/10.5281/zenodo.16760254 (2025).

1119

1120

1121 **ACKNOWLEDGMENTS**

1122 We thank Cheryl Maduro and Büşra Göynük for technical support in generating the cell
1123 lines, the VIB FACS Core for their assistance in sorting cells, the KU Leuven Genomics Core
1124 for assistance with sequencing, as well as the Vlaams Supercomputer Centrum for their
1125 computational resources. We thank Björn Reinius and our colleagues for many helpful
1126 discussions. The V.P. laboratory is supported by the Research Foundation-Flanders (FWO
1127 grants G0C9320N and G0B4420N to V.P.), KU Leuven Research Fund (C1 grant
1128 C14/21/119 to V.P.), and Pandarome project 40007487 (G0I7822N) (funded by the FWO
1129 and F.R.S.-FNRS) under the Excellence of Science (EOS) program. R.N.A is supported by
1130 FWO fellowship (11L0724N). J.B. is supported by the Oncode Institute. S.M. is supported
1131 by ZonMW-Top subsidy (40008129815046).

AUTHOR CONTRIBUTIONS

Conceptualization: V.P., R.N.A., J.G., B.F.T, J.B., H.M.B., C.G.
Data curation: R.N.A., B.F.T., J.B., S.M.
Formal analysis: R.N.A., B.F.T., J.B., S.P., W.F.J.I, J.A.A.D
Funding acquisition: V.P., J.G.
Investigation: V.P., R.N.A., J.G., B.F.T, J.B., H.M.B., C.G.
Methodology: R.N.A., B.F.T., J.B., S.P., W.F.J.I, J.A.A.D
Project administration: V.P., J.G.
Resources: V.P., J.G., J.A.A.D
Software: V.P., J.G., J.A.A.D
Supervision: V.P., J.G., H.M.B., C.G
Validation: R.N.A., B.F.T., J.B.
Visualization: R.N.A., J.B., B.F.T
Writing, reviewing and editing of the manuscript: V.P., R.N.A., J.G., B.F.T, J.B., H.M.B., C.G.

COMPETING INTERESTS

KU Leuven in Belgium has filed an international patent application (PCT/EP2023/073949) for methods to create ExM cells from naive human PSCs. V.P. is one of the inventors of this patent. The remaining authors declare no competing interests.

1153 **FIGURE LEGENDS**

1154 **Figure 1. Transcriptional dosage compensation of X-linked genes in mouse**
1155 **pluripotent stem cell lines with X-chromosome monosomy.**

1156 **a.** Schematic depiction of cells with different sex chromosome complements (XX, XY, and
1157 XO) and the corresponding expected upregulation status of the X chromosome (gray: not
1158 upregulated, green: upregulated).

1159 **b, c.** Violin plots of the mean normalized gene expression from the *Mus* (**b**) and *Cast* (**c**)
1160 allele of all expressed X-linked genes in $X^{Cast}X^{Mus}$ (green), $X^{Cast}O^{Mus}$ (blue), $X^{Mus}O^{Cast}$ (orange),
1161 and $X^{Mus}Y$ (yellow) cells. Dashed line indicates the mean value of XX cells, serving as a
1162 reference line for expected expression without upregulation. Each dot represents a cell. P-
1163 values were calculated via the Tukey HSD test (two-sided, with Tukey-Kramer correction for
1164 multiple comparisons).

1165 **d, e.** Violin plots of the mean X:A ratio of the *Mus* (**d**) and *Cast* (**e**) allele in $X^{Cast}X^{Mus}$, $X^{Cast}O^{Mus}$,
1166 $X^{Mus}O^{Cast}$, and $X^{Mus}Y$ cells. The dashed line indicates the mean value of XX cells, serving as a
1167 reference line for expected expression without upregulation. Each dot represents a cell. P-
1168 values were calculated using the Tukey HSD test (two-sided, with Tukey-Kramer correction
1169 for multiple comparisons).

1170 **f**. Normalized expression in $X^{Cast}X^{Mus}$ iPSCs of genes annotated as upregulated (in XO and
1171 XY cells, n=103, green) or non-upregulated (n=168, gray). P-value was calculated using a
1172 two-sided Student's t-test.

1173 **g**. Schematic overview of the experimental set-up used to generate allele-specific ChIP-seq
1174 data[57].

1175 **h-i**. Line plots showing the promoter enrichment of repressive (**h**) and active (**i**) histone
1176 modifications on the active *Cast* allele during XCI inactivation, and thus XCU induction.
1177 Promoter enrichment was quantified as the mean counts per 10 million (CP10M) in the 1kb
1178 region upstream of the TSS (as shown for the 24 hour time point in **Supplementary Fig. 3d**
1179 **and 4c**). Mean enrichment is plotted for the promoters of upregulated (green) and non-
1180 upregulated (gray) genes separately, with shaded areas indicating the standard error. P-
1181 values comparing enrichment at 0 and 24 hours were calculated using two-sided paired t-
1182 tests, corrected for multiple testing with the Benjamini-Hochberg method, and shown to the
1183 right of each gene set.

1184 **Figure 2. Large heterozygous segmental deletions do not result in global XCU *in trans*.**
1185 **a**. Schematic depiction of the XCU center hypothesis. Gray denotes an X chromosome that
1186 is not upregulated, while green indicates an upregulated X chromosome.
1187 **b.** Schematic overview of the deletion cell lines used in the scRNA-seq experiment and their
1188 respective sex chromosome karyotypes.
1189 **c.** Heatmap of all scRNA-seq data for X-linked genes, ordered by chromosomal position,
1190 grouped by cell line, and colored by log-transformed normalized expression values for each
1191 allele. The position of genes *Tfe3*, *Zic3*, *Dusp9*, and *Nr0b1* are highlighted, as these genes
1192 denote the start and end positions of each deletion.
1193 **d**. Schematic depiction of the XCU center hypothesis, such that deletion of a region of one
1194 X chromosome induces transcriptional upregulation for genes located outside of the
1195 deletion region *in trans*.
1196 **e-g**. Violin plots separated by cell line showing the mean gene expression from the non-
1197 deleted allele for the genes located outside of the regions of Deletion 1 (**e**, *Cast* allele),
1198 Deletion 2 (**f**, *Cast* allele) and Deletion 3 (**g**, *Mus* allele). The dashed line indicates the mean
1199 value of XX cells, serving as a reference line for expected expression without upregulation.
1200 Each dot represents a cell. P-values calculated via the Tukey HSD test (two-sided, with
1201 Tukey-Kramer correction for multiple comparisons, ns - not significant).

1202 **Figure 3. The X chromosome does not contain an XCU center.**
1203 **a.** Schematic overview of the deletions generated for the bulk RNA-seq experiment, as well
1204 as deletions 1, 2, and 3. All deletions were introduced in hybrid (*Mus/Cast*) ESC lines with a
1205 heterozygous *Rnf12* deletion on the *Mus* allele. Deletion G was found to be a recombination
1206 event rather than a deletion, and has been omitted from all subsequent analyses.
1207 **b.** Heatmap of all X-linked genes ordered by chromosomal position, grouped by cell line,
1208 and colored by log-transformed normalized expression values for each allele. The expected
1209 deleted region for each deletion line is highlighted on the right side of the heatmap.
1210 **c.** Scatter plots separated by deletion showing the mean copy number-corrected
1211 expression levels of genes located outside each deletion for $X^{Cast}X^{Mus}$, $X^{Cast}O^{Mus}$, and cells
1212 with the corresponding deletion. Each dot represents a biological replicate (independent
1213 clones). The dashed line represents the average level from the XX samples, serving as a
1214 reference line for expected expression without upregulation. Note that the gene sets differ
1215 between panels, resulting in varying expression levels in $X^{Cast}X^{Mus}$ and $X^{Cast}O^{Mus}$ across
1216 panels. **d.** Scatter plots separated by deletion showing the $\log_2$ fold change in copy
1217 number-corrected expression levels of replicates of $X^{Cast}X^{Mus}$, $X^{Cast}O^{Mus}$, and cells with the
1218 corresponding deletion, relative to the mean $X^{Cast}X^{Mus}$ levels per gene. Only genes
1219 upregulated in the $X^{Cast}O^{Mus}$ cells and located outside each respective deletion are shown
1220 (n=110, 115, 93, 117, 112, 73, 113, 119, 118, 122, 95, 116, 116). Each dot represents a
1221 gene, and the solid line indicates the median $\log_2$ fold change. P-values comparing mean
1222 expression between genotypes were calculated using two-sided paired t-tests, and
1223 corrected for multiple testing with the Bonferroni method (ns - not significant).

1224 **Figure 4. Dosage compensation by transcriptional upregulation occurs *in trans* for**
1225 **genes within regions of X-chromosome monosomy.**
1226 **a.** Schematic depiction of gene-by-gene regulation of dosage compensation. Gray denotes
1227 an X chromosome that is not upregulated, while green indicates an upregulated X
1228 chromosome.
1229 **b-d.** Violin plots separated by cell line showing the mean gene expression from the non-
1230 deleted allele for the genes located inside the regions of Deletion 1 (**b**, *Cast* allele), Deletion
1231 2 (**c**, *Cast* allele) and Deletion 3 (**d**, *Mus* allele). The dashed line indicates the mean value of
1232 XX cells, serving as a reference line for expected expression without upregulation. Each dot
1233 represents a cell. P-values were calculated via the Tukey HSD test (two-sided, with Tukey-
1234 Kramer correction for multiple comparisons).
1235 **e.** Scatter plots separated by deletion showing the mean copy number-corrected
1236 expression levels of genes located within each deletion for $X^{Cast}X^{Mus}$, $X^{Cast}O^{Mus}$, and cells with
1237 the corresponding deletion. Each dot represents a biological replicate (independent clones).
1238 The dashed line indicates the average level from the XX samples, serving as a reference line
1239 for expected expression without upregulation. Deletion I did not contain sufficient
1240 expressed genes and has been omitted.
1241 **f.** Scatter plots separated by deletion showing the $\log_2$ fold change in copy number-
1242 corrected expression levels of replicates of $X^{Cast}X^{Mus}$, $X^{Cast}O^{Mus}$, and cells with the
1243 corresponding deletion, relative to the mean $X^{Cast}X^{Mus}$ levels per gene. Only genes
1244 upregulated in the $X^{Cast}O^{Mus}$ cells and located within each respective deletion are shown
1245 (n=15, 10, 32, 8, 13, 52, 12, 6, 7, 3, 30, 9, 9). Each dot represents a gene, and the solid line
1246 indicates the median $\log_2$ fold change.
1247 **g.** Heatmap showing the fold change in expression of upregulated genes identified from the
1248 allelic single-cell analysis between $X^{monosomy}$ and $X^{Cast}X^{Mus}$. Fold change is calculated between
1249 *Cast* expression from either $X^{Cast}O^{Mus}$, Deletion 1, or Deletion 2 cells and total allelic
1250 expression divided by 2 from XX cells, or *Mus* expression from $X^{Mus}O^{Cast}$, $X^{Mus}Y$, or Deletion
1251 3 cells and total allelic expression divided by 2 from $X^{Cast}X^{Mus}$ cells.
1252 **h.** Bar plot of the relative RNA expression of the gene *Pdzd4* in XX wild type ($X^{Cast}X^{Mus}$, n=3),
1253 *Rnf12*$^{+/-}$ parental line (*Rnf12*$^{+/-}$, n=3), XO ($X^{Cast}O^{Mus}$, n=2), and 4 different *Rnf12*$^{+/-}$*Pdzd4*$^{+/-}$
1254 clones for both the *Mus* (blue) and *Cast* (red) allele. Average expression ± standard
1255 deviation, each dot represents a biological replicate (for XO and *Rnf12*$^{+/-}$*Pdzd4*$^{+/-}$ from
1256 independent clones).

1257 **Figure 5. Dosage compensation is induced by transcriptional upregulation *in trans***
1258 **within regions of monosomic expression on chromosome 3.**
1259 **a.** Schematic depiction of the location of the *Xist* transgene on chromosome 3[61]. After 24
1260 hours of dox treatment, *Xist* coats the *Cast* chromosome 3, reducing gene expression.
1261 **b.** Overview of the genomic location of genes showing reduced expression on the Cast
1262 allele of chromosome 3 (black lines), as well as the location of the left border (red line) of the
1263 region defined as being inactive (green area) and the site of the *Xist* transgene (blue line).
1264 **c-e.** Plot of median normalized expression from the *Cast* (**c**) or *Mus* (**d**, **e**) allele of genes
1265 inside (**c**, **e**) or outside (**d**) the region with reduced gene expression for both control (-dox)
1266 and treated (+dox) conditions. Dashed lines indicate the mean levels per condition. P-
1267 values were calculated via the two-sided Student's t-test (ns - not significant). Each dot
1268 represents a biological replicate.

1269 **Figure 6. Protein-level dosage compensation is induced within regions of monosomic**
1270 **expression on the X chromosome.**
1271 **a.** Copy number-corrected protein abundance for all X-linked proteins in $X^{Cast}X^{Mus}$, $X^{Mus}Y$ and
1272 $X^{Cast}O^{Mus}$ ESCs. The mean (of n=127 proteins) per biological replicate from a single clone is
1273 depicted with a dot, with the corresponding 95% confidence intervals shown as error bars.
1274 The dashed line indicates the mean value of $X^{Cast}X^{Mus}$ cells, serving as a reference line for
1275 expected expression without upregulation.
1276 **b, c.** Volcano plots displaying the differential protein expression analysis of X-linked
1277 proteins between $X^{Mus}Y$ and $X^{Cast}X^{Mus}$ samples (**b**) and between $X^{Cast}O^{Mus}$ and XX samples (**c**)
1278 (n=3). Each dot represents a protein. P-values were calculated from copy number-corrected
1279 protein quantifications using Tukey's HSD test (two-sided, with Tukey-Kramer correction for
1280 multiple comparisons). Significantly up- and downregulated proteins are highlighted in red
1281 and blue, respectively ($\alpha < 0.05$, $\log_2$(fold change) > 0.5 or < -0.5, respectively).
1282 **d**. Barplot displaying the proportion of upregulated genes per chromosome. The X
1283 chromosome is highlighted in green.
1284 **e**. Barplot showing the proportion of complex-forming proteins in the upregulated (green)
1285 and non-upregulated (gray) protein lists. P-values were calculated via the Chi-square test.
1286 **f.** Scatter plot showing the correlation between upregulation at RNA and protein level. Each
1287 dot represents a gene/protein. For both levels, the fold change between $X^{Cast}O^{Mus}$ and half of
1288 the $X^{Cast}X^{Mus}$ level is shown for each gene. Genes are colored according to their upregulation
1289 status at both (orange), either (blue or green) or neither (gray) levels. Shaded area indicates
1290 95% confidence interval.
1291 **g, h.** Scatter plots separated by region showing the mean copy number-corrected
1292 abundance levels of proteins encoded by genes located outside (**g**) and within (**h**) region E
1293 and K for $X^{Cast}X^{Mus}$, $X^{Mus}Y$, $X^{Cast}O^{Mus}$ ESCs and ESCs with the corresponding deletion. Each
1294 dot represents a biological replicate from a single clone. The dashed line represents the
1295 average abundance levels from the $X^{Cast}X^{Mus}$ samples.
1296 i. Heatmap showing the z-scores of copy-number corrected protein quantifications for X-
1297 linked proteins upregulated in both $X^{Cast}Y$ and $X^{Cast}O^{Mus}$ samples compared to $X^{Cast}X^{Mus}$.
1298 Proteins are ordered by genomic locations, with deletions E and K highlighted in light blue
1299 and pink, respectively. Proteins expected to be upregulated are highlighted with a box.

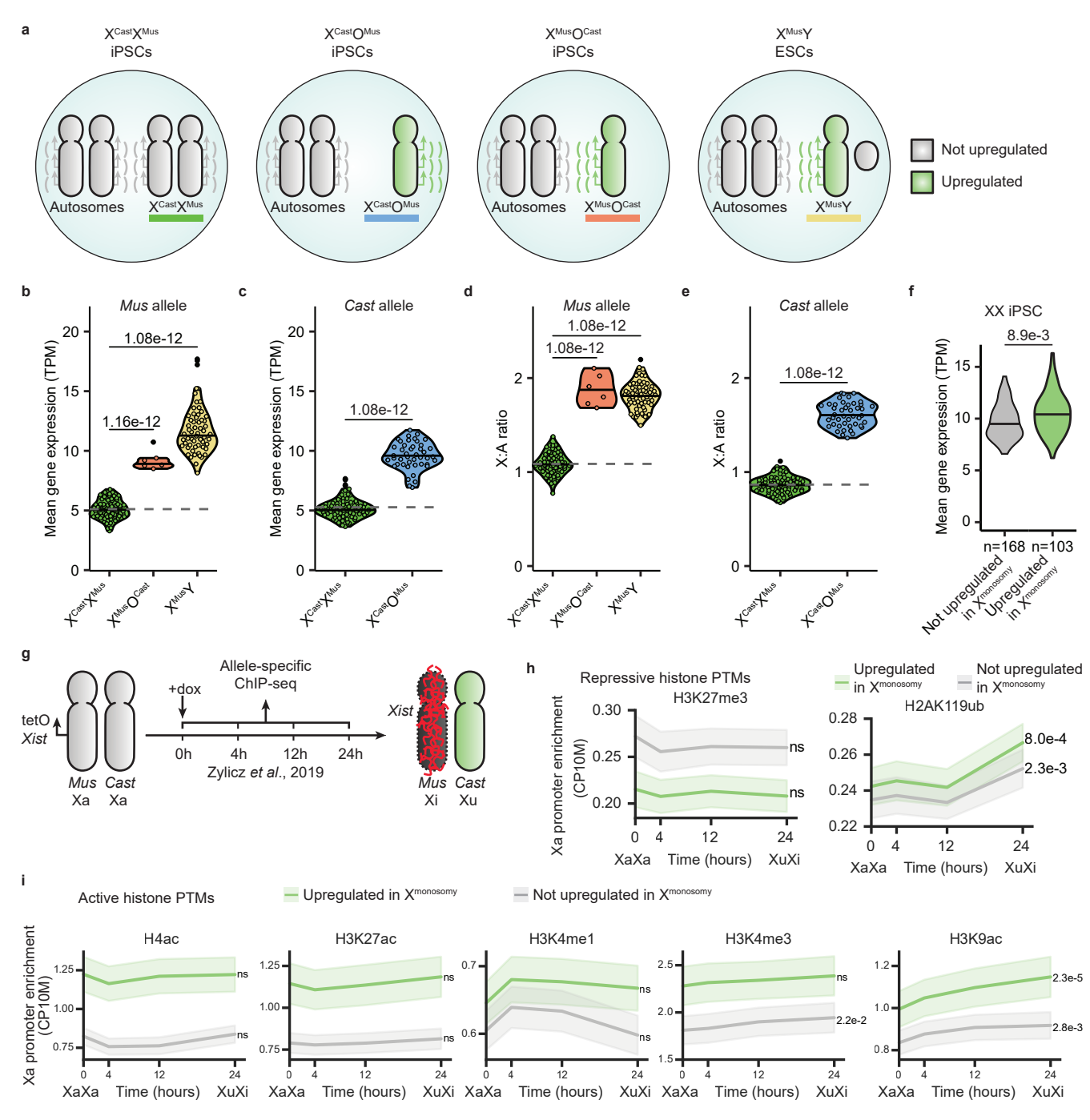
a
XCastXMus iPSCs
XCastOMus iPSCs
XMusOCast iPSCs
XMusY ESCs
Autosomes
XCastXMus
XCastOMus
XMusOCast
XMusY
Not upregulated
Upregulated
b
Mus allele
Mean gene expression (TPM)
1.08e-12
1.16e-12
c
Cast allele
1.08e-12
d
Mus allele
X:A ratio
1.08e-12
1.08e-12
e
Cast allele
1.08e-12
f
XX iPSC
8.9e-3
n=168
n=103
Not upregulated in Xmonosomy
Upregulated in Xmonosomy
g
tetO
Xist
Mus Xa
Cast Xa
+dox
Allele-specific ChIP-seq
0h
4h
12h
24h
Zylicz et al., 2019
Mus Xi
Cast Xu
h
Repressive histone PTMs
H3K27me3
Xa promoter enrichment (CP10M)
ns
ns
XaXa
Time (hours)
XuXi
Upregulated in Xmonosomy
Not upregulated in Xmonosomy
H2AK119ub
8.0e-4
2.3e-3
i
Active histone PTMs
H4ac
H3K27ac
H3K4me1
H3K4me3
H3K9ac
2.2e-2
2.3e-5
2.8e-3

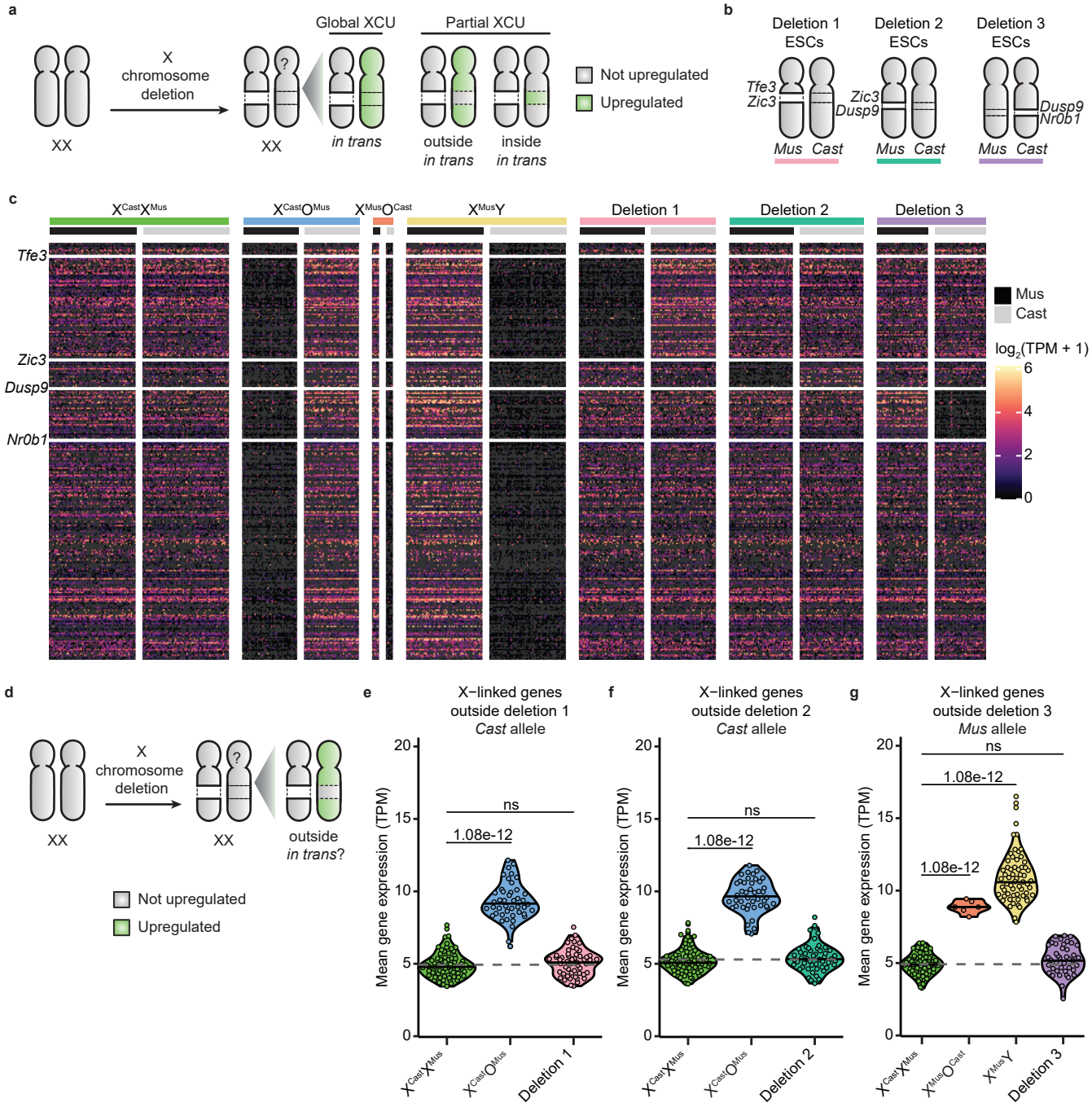
a
X chromosome deletion
XX
XX
Global XCU
Partial XCU
in trans
outside in trans
inside in trans
Not upregulated
Upregulated
b
Deletion 1 ESCs
Deletion 2 ESCs
Deletion 3 ESCs
Tfe3
Zic3
Zic3
Dusp9
Dusp9
Nr0b1
Mus Cast
Mus Cast
Mus Cast
c
XCastXMus
XCastOMus
XMusOCast
XMusY
Deletion 1
Deletion 2
Deletion 3
Tfe3
Zic3
Dusp9
Nr0b1
Mus
Cast
log2(TPM + 1)
6
4
2
0
d
X chromosome deletion
XX
XX
outside in trans?
Not upregulated
Upregulated
e
X−linked genes outside deletion 1
Cast allele
Mean gene expression (TPM)
ns
1.08e-12
XCastXMus
XCastOMus
Deletion 1
f
X−linked genes outside deletion 2
Cast allele
Mean gene expression (TPM)
ns
1.08e-12
XCastXMus
XCastOMus
Deletion 2
g
X−linked genes outside deletion 3
Mus allele
Mean gene expression (TPM)
ns
1.08e-12
1.08e-12
XCastXMus
XMusOCast
XMusY
Deletion 3

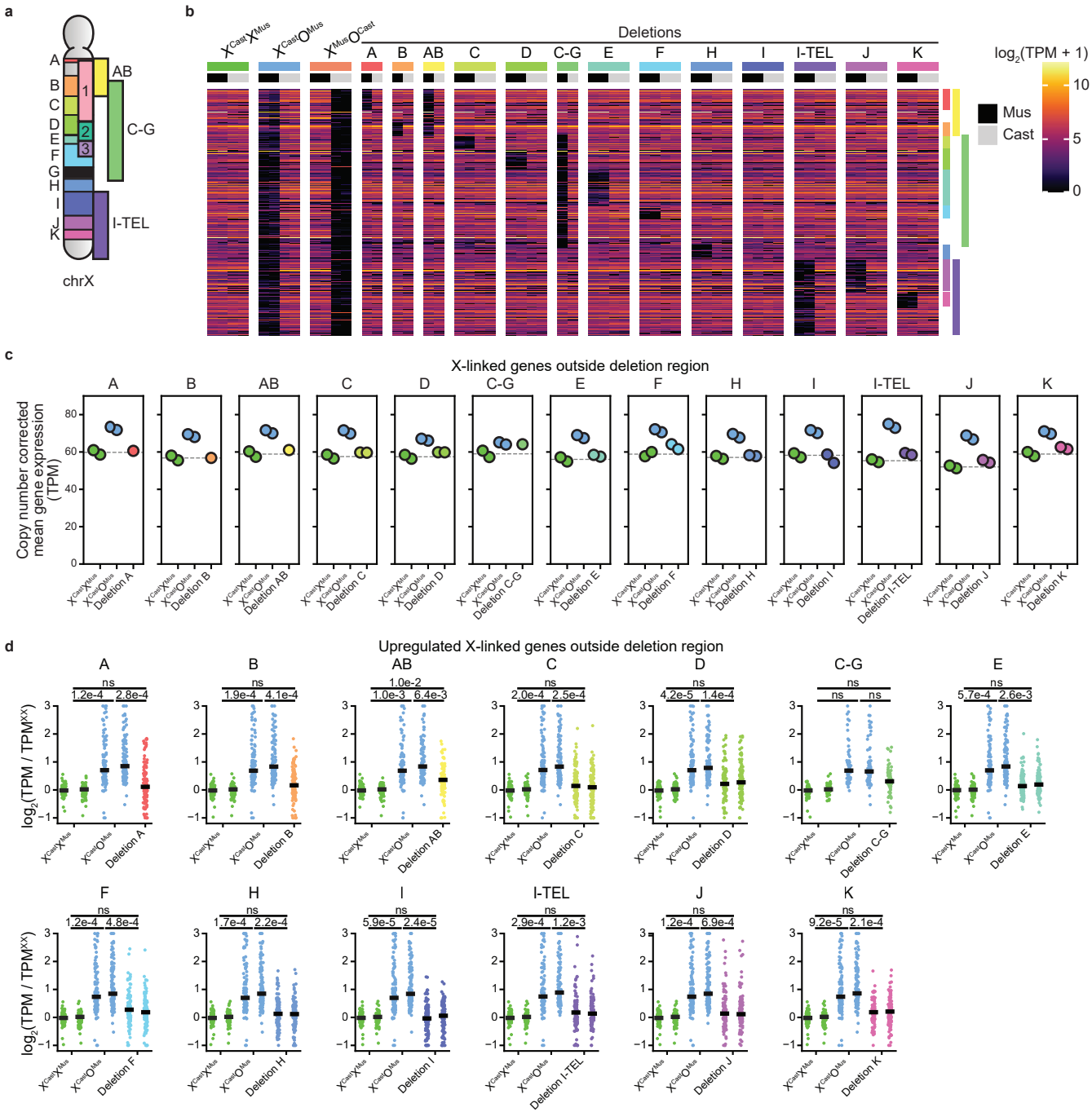
a
A
B
C
D
E
F
G
H
I
J
K
1
2
3
AB
C-G
I-TEL
chrX
b
Deletions
A
B
AB
C
D
C-G
E
F
H
I
I-TEL
J
K
log2(TPM + 1)
Mus
Cast
c
X-linked genes outside deletion region
Copy number corrected mean gene expression (TPM)
Deletion A
Deletion B
Deletion AB
Deletion C
Deletion D
Deletion C-G
Deletion E
Deletion F
Deletion H
Deletion I
Deletion I-TEL
Deletion J
Deletion K
d
Upregulated X-linked genes outside deletion region
log2(TPM / TPMXX)
ns
1.2e-4
2.8e-4
1.9e-4
4.1e-4
1.0e-2
1.0e-3
6.4e-3
2.0e-4
2.5e-4
4.2e-5
1.4e-4
5.7e-4
2.6e-3
1.2e-4
4.8e-4
1.7e-4
2.2e-4
5.9e-5
2.4e-5
2.9e-4
1.2e-3
1.2e-4
6.9e-4
9.2e-5
2.1e-4

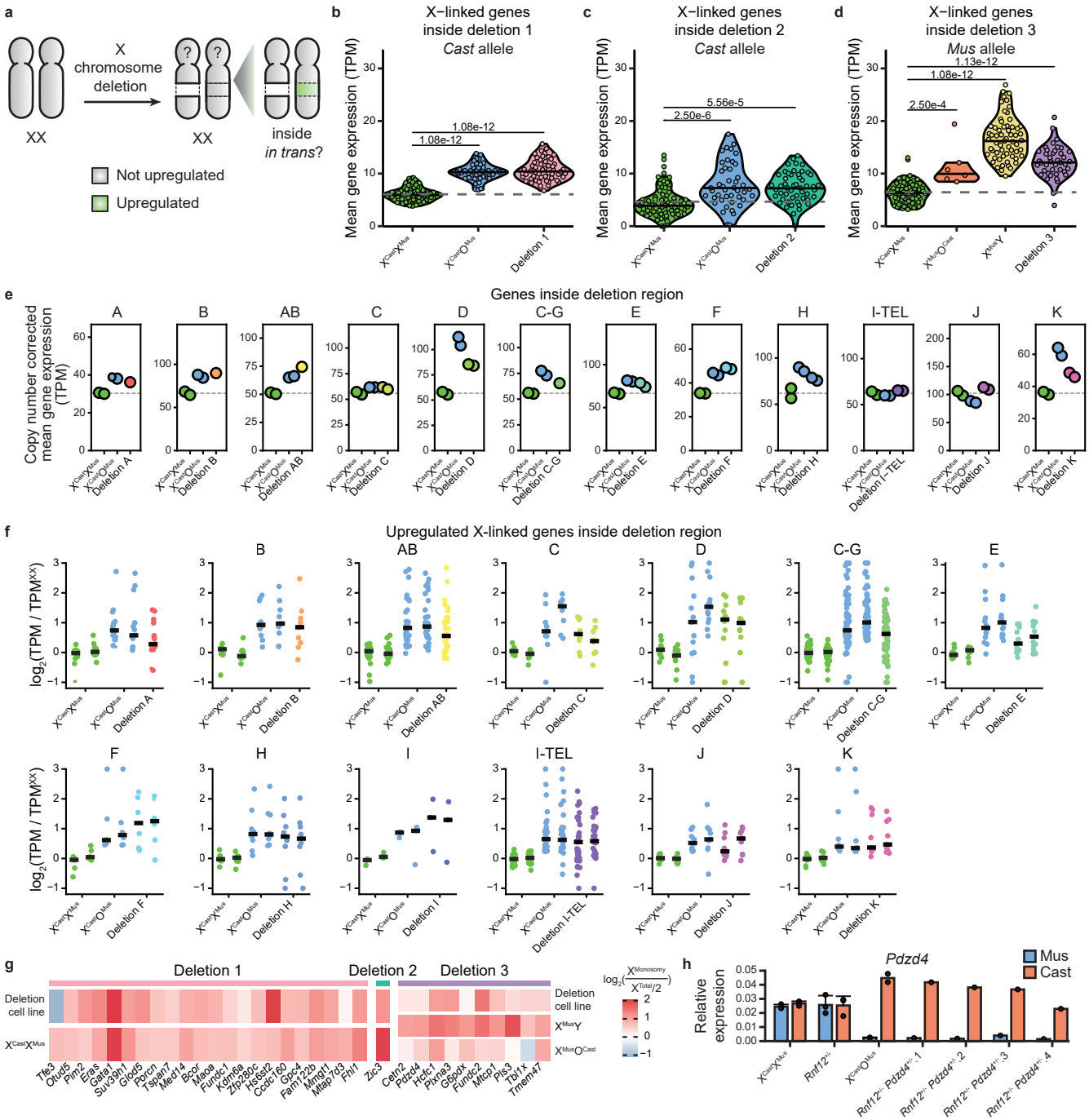
a
X chromosome deletion
XX
XX
inside in trans?
Not upregulated
Upregulated
b
X−linked genes inside deletion 1
Cast allele
Mean gene expression (TPM)
1.08e-12
1.08e-12
Deletion 1
c
X−linked genes inside deletion 2
Cast allele
5.56e-5
2.50e-6
Deletion 2
d
X−linked genes inside deletion 3
Mus allele
1.13e-12
1.08e-12
2.50e-4
Deletion 3
e
Genes inside deletion region
Copy number corrected mean gene expression (TPM)
A
B
AB
C
D
C-G
E
F
H
I-TEL
J
K
f
Upregulated X-linked genes inside deletion region
log2(TPM / TPMXX)
g
Deletion 1
Deletion 2
Deletion 3
Deletion cell line
Tfe3
Otud5
Pim2
Eras
Gata1
Suv39h1
Gldc
Porcn
Tsaan7
Med14
Bcor
Maoa
Fundc1
Kdm6a
Zfp280c
Hs6st2
Ccdc160
Gpc4
Fam122b
Mmgt1
Mtap7d3
Fhl1
Zic3
Cetn2
Pdzd4
Hcfc1
Plxna3
Gpodx
Fundc2
Mtcp1
Pls3
Tbl1x
Tmem47
h
Pdzd4
Mus
Cast
Relative expression
Rnf12+/-
Rnf12+/- Pdzd4+/- 1
Rnf12+/- Pdzd4+/- 2
Rnf12+/- Pdzd4+/- 3
Rnf12+/- Pdzd4+/- 4

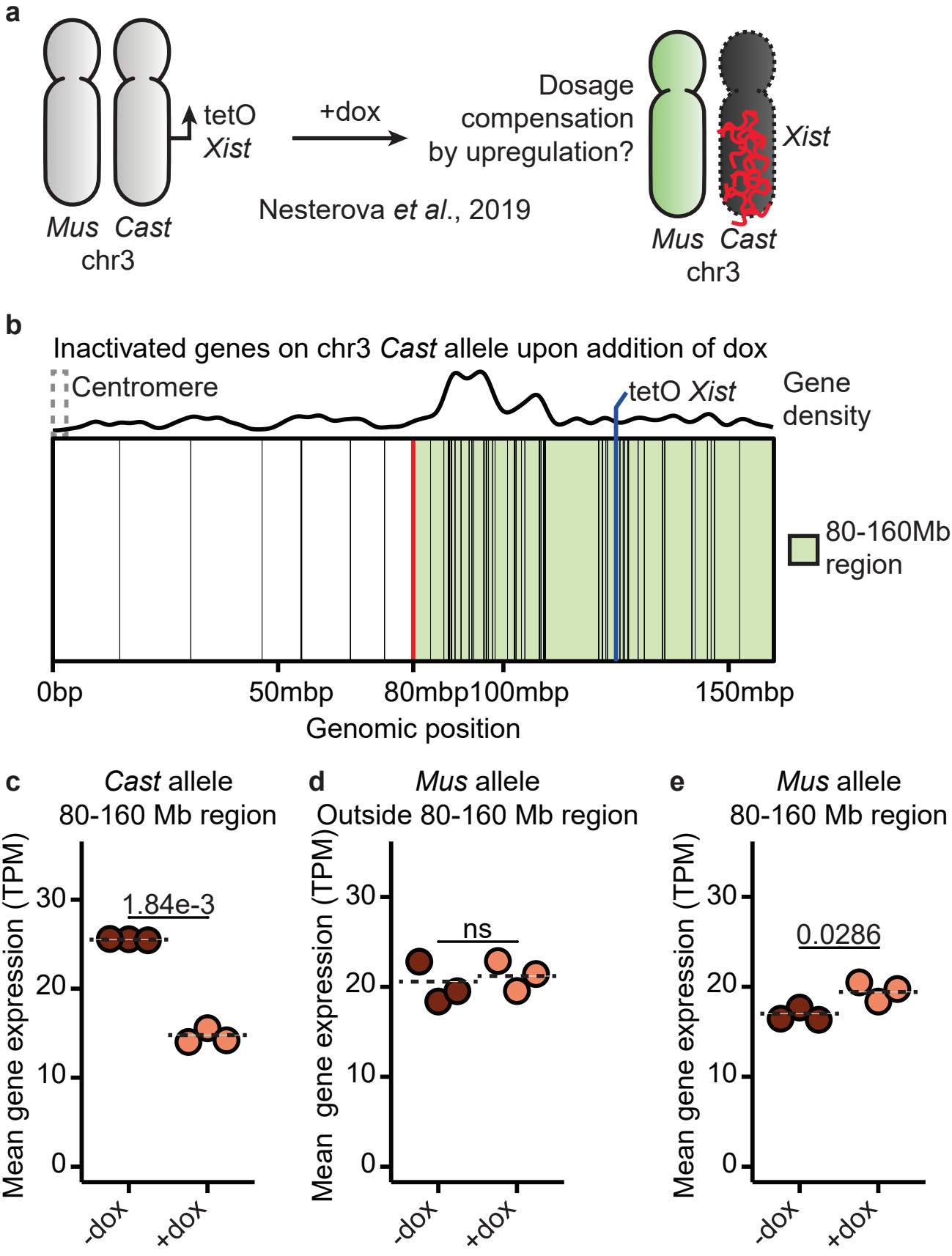
a
tetO
Xist
Mus Cast
chr3
+dox
Dosage
compensation
by upregulation?
Xist
Mus Cast
chr3
Nesterova et al., 2019
b
Inactivated genes on chr3 Cast allele upon addition of dox
Centromere
tetO Xist
Gene
density
80-160Mb
region
0bp
50mbp
80mbp
100mbp
150mbp
Genomic position
c
Cast allele
80-160 Mb region
Mean gene expression (TPM)
1.84e-3
-dox
+dox
d
Mus allele
Outside 80-160 Mb region
Mean gene expression (TPM)
ns
-dox
+dox
e
Mus allele
80-160 Mb region
Mean gene expression (TPM)
0.0286
-dox
+dox

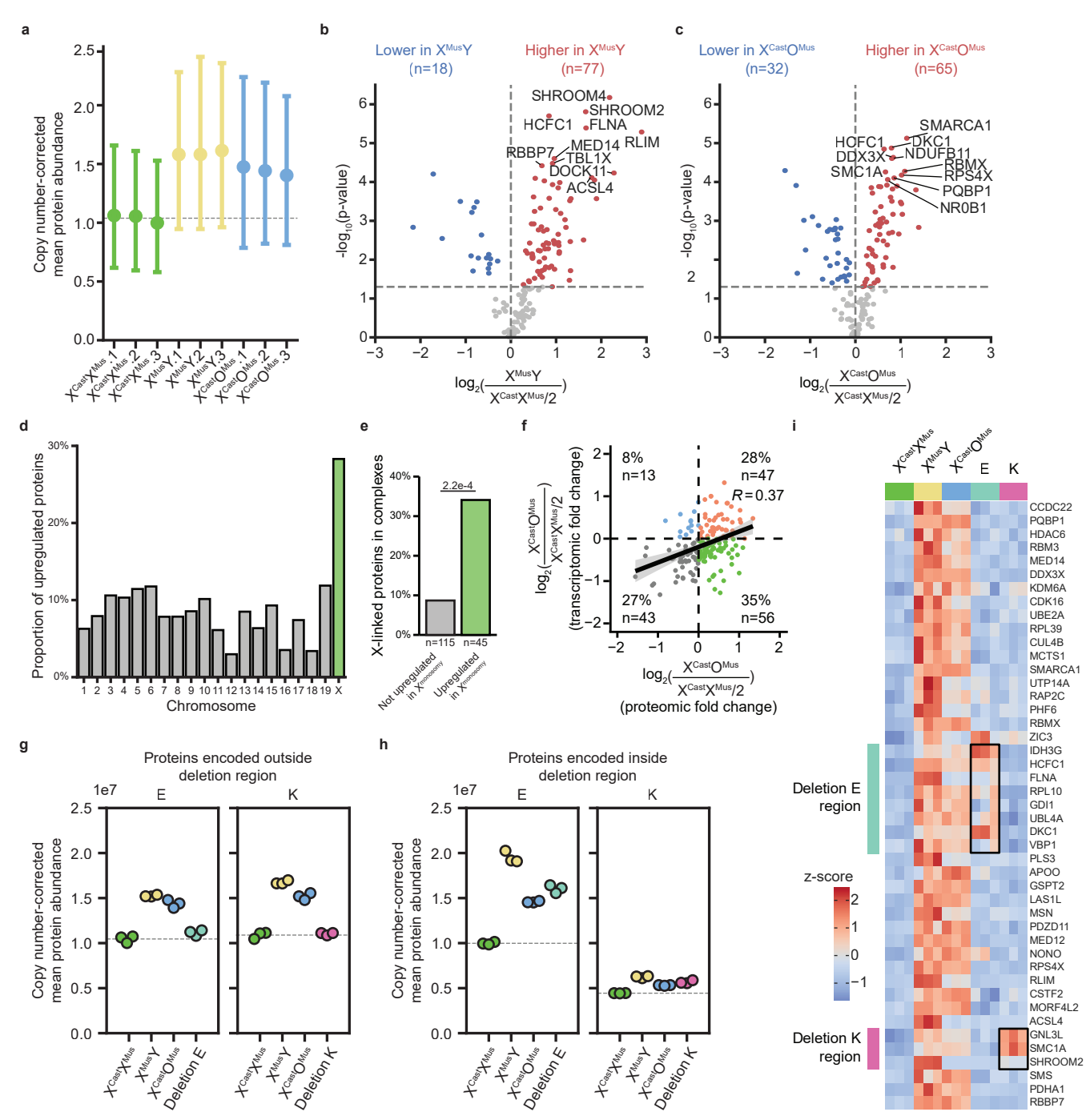

a
Copy number-corrected mean protein abundance
b
Lower in XMusY (n=18)
Higher in XMusY (n=77)
SHROOM4
SHROOM2
HCFC1
FLNA
RLIM
RBBP7
MED14
TBL1X
DOCK11
ACSL4
-log10(p-value)
log2(XMusY / XCastXMus/2)
c
Lower in XCastOMus (n=32)
Higher in XCastOMus (n=65)
SMARCA1
HOFC1
DKC1
DDX3X
NDUFB11
SMC1A
RBMX
RPS4X
PQBP1
NR0B1
-log10(p-value)
log2(XCastOMus / XCastXMus/2)
d
Proportion of upregulated proteins
Chromosome
e
X-linked proteins in complexes
2.2e-4
n=115
n=45
Not upregulated in Xmonosomy
Upregulated in Xmonosomy
f
8% n=13
28% n=47
R=0.37
27% n=43
35% n=56
log2(XCastOMus / XCastXMus/2) (transcriptomic fold change)
log2(XCastOMus / XCastXMus/2) (proteomic fold change)
i
E
K
CCDC22
PQBP1
HDAC6
RBM3
MED14
DDX3X
KDM6A
CDK16
UBE2A
RPL39
CUL4B
MCTS1
SMARCA1
UTP14A
RAP2C
PHF6
RBMX
ZIC3
IDH3G
HCFC1
FLNA
RPL10
GDI1
UBL4A
DKC1
VBP1
PLS3
APOO
GSPT2
LAS1L
MSN
PDZD11
MED12
NONO
RPS4X
RLIM
CSTF2
MORF4L2
ACSL4
GNL3L
SMC1A
SHROOM2
SMS
PDHA1
RBBP7
Deletion E region
Deletion K region
z-score
g
Proteins encoded outside deletion region
1e7
E
K
Copy number-corrected mean protein abundance
Deletion E
Deletion K
h
Proteins encoded inside deletion region
1e7
E
K
Copy number-corrected mean protein abundance
Deletion E
Deletion K